Annual Report

Hydrospheric Atmospheric Research Center (HyARC)

Nagoya University

2008

Annual Report

Hydrospheric Atmospheric Research Center (HyARC)

2008

NAGOYA UNIVERSITY

Contents

Foreword

The Hydrospheric Atmospheric Research Center (HyARC) at Nagoya University was established eight years ago to promote research on the global water cycle, one of the primary components of the Earth system. Research on the global water cycle requires strong and extensive collaboration among science and application communities, and hence HyARC functions as an inter-university collaborative system, in many ways unique in the world.

HyARC has initiated numerous projects and activities. Prominent among these is the International Project Office of the Global Energy and Water Cycle Experiment (GEWEX) Asian Monsoon Experiment (GAME), led by Prof. T. Yasunari, and its various follow-on projects. Additional work has been supported by the following: Grants-in-Aid for Scientific Research; Core Research for Evolutional Science and Technology (CREST) of the Japan Science and Technology Corporation (JST); Global Environment Research Fund; Innovative Program of Climate Change Projection for the 21st Century; and more. In addition, funding from the Ministry of Education, Culture, Sports, Science and Technology, Japan, supported construction of a multi-parameter radar system to study water circulation, and funding from the Inter-University Project supported a virtual laboratory for study of the earth's climate diagnostics.

HyARC has also collaborated with numerous institutions, such as the Research Institute of Humanity and Nature (RIHN) and the National Institute of Information and Communication Technology (NICT). As partial contribution to the UNESCO International Hydrology Programme (IHP), HyARC has conducted training courses, funded by the Japan Trust; this year's course was on satellite remote sensing of atmospheric constituents.

In selecting projects and activities, HyARC considers project feasibility, significance, and collaboration requirements. We currently fund four research center projects and one workshop. Although HyARC's permanent staff numbers only 11 (4 professors, 4 associate professors, and 3 assistant professors), we also support many postdoctoral candidates in active research. In addition, we have accepted graduate students in the Department of Environmental Studies.

Nagoya University has adopted a flexible management system that emphasizes accountability yet encourages research publications and outreach programs. Accordingly, and spurred by comments from an outside evaluation committee, we herewith propose to establish a large-scale national/international facility, and a new organization to address its social requirements.

UYEDA Hiroshi
Director
Hydrospheric Atmospheric Research Center

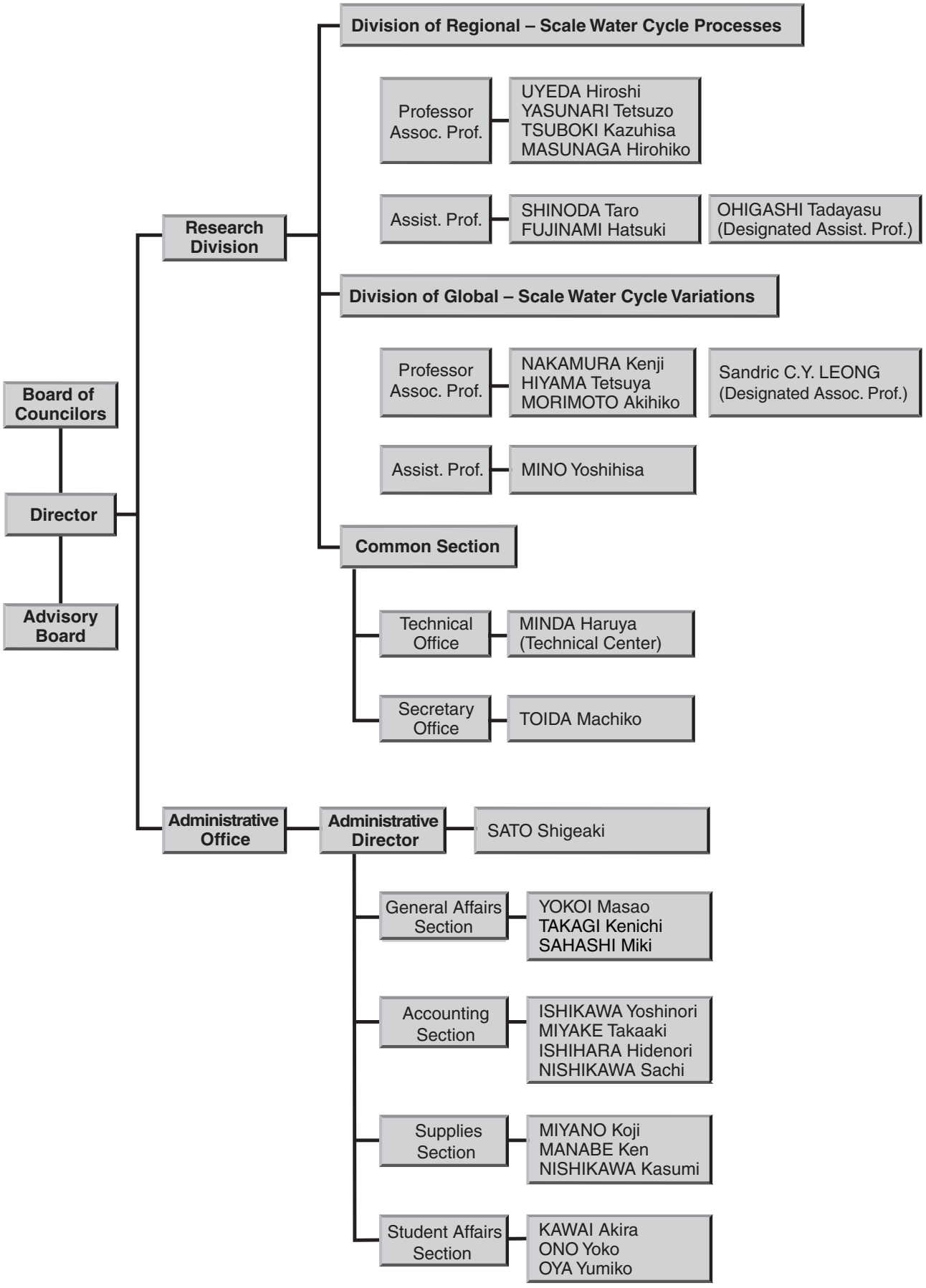
Board of Councilors
Director
Advisory Board
Research Division
Division of Regional – Scale Water Cycle Processes
Professor
Assoc. Prof.
UYEDA Hiroshi
YASUNARI Tetsuzo
TSUBOKI Kazuhisa
MASUNAGA Hirohiko
Assist. Prof.
SHINODA Taro
FUJINAMI Hatsuki
OHIGASHI Tadayasu
(Designated Assist. Prof.)
Division of Global – Scale Water Cycle Variations
Professor
Assoc. Prof.
NAKAMURA Kenji
HIYAMA Tetsuya
MORIMOTO Akihiko
Sandric C.Y. LEONG
(Designated Assoc. Prof.)
Assist. Prof.
MINO Yoshihisa
Common Section
Technical Office
MINDA Haruya
(Technical Center)
Secretary Office
TOIDA Machiko
Administrative Office
Administrative Director
SATO Shigeaki
General Affairs Section
YOKOI Masao
TAKAGI Kenichi
SAHASHI Miki
Accounting Section
ISHIKAWA Yoshinori
MIYAKE Takaaki
ISHIHARA Hidenori
NISHIKAWA Sachi
Supplies Section
MIYANO Koji
MANABE Ken
NISHIKAWA Kasumi
Student Affairs Section
KAWAI Akira
ONO Yoko
OYA Yumiko

Administration

Board of Councilors

UYEDA Hiroshi: *Director, Prof., Hydrospheric Atmospheric Research Center*
YASUNARI Tetsuzo: *Prof., Hydrospheric Atmospheric Research Center*
NAKAMURA Kenji: *Prof., Hydrospheric Atmospheric Research Center*
TANAKA Kentaro: *Prof., Graduate School of Science*
TSUJIMOTO Tetsuro: *Prof., Graduate School of Engineering*
HATTORI Shigeaki: *Prof., Graduate School of Bioagricultural Sciences*
KANZAWA Hiroshi: *Prof., Graduate School of Environmentral Studies*
FUJII Ryoichi: *Prof., Solar-Terrestrial Environment Laboratory*

Advisory Board

● **Members from Nagoya Unisversity**

UYEDA Hiroshi: *Director, Prof., Hydrospheric Atmosphric Research Center*
YASUNARI Tetsuzo: *Prof., Hydrospheric Atmospheric Research Center*
NAKAMURA Kenji: *Prof., Hydrospheric Atmosphric Research Center*
TSUBOKI Kazuhisa: *Assoc. Prof., Hydrospheric Atmosphric Research Center*
MASUNAGA Hirohiko: *Assoc. Prof., Hydrospheric Atmosphric Research Center*
HIYAMA Tetsuya: *Assoc. Prof., Hydrospheric Atmosphric Research Center*
MORIMOTO Akihiko: *Assoc. Prof., Hydrospheric Atmosphric Research Center*
MIZUTANI Norimi: *Prof., Graduate School of Engineering*
OHTA Takeshi: *Prof., Graduate School of Bioagricultural Sciences*
YAMAGUCHI Yasushi: *Prof., Graduate School of Environment Studies*
MATSUMI Yutaka: *Prof., Solar-Terrestrial Environment Laboratory*

● **Members outside Nagoya University**

FUJIYOSHI Yasushi: *Prof., Institute of Low Temparature Science, Hokkaido University*
HANAWA Kimio: *Prof., Graduate School of Science, Tohoku University*
SUMI Akimasa: *Prof., Integrated Research System for Sustainability Science, The University of Tokyo*
FUKUSHIMA Yoshihiro: *Prof., Tottori University of Environmental Studies*
YAMANAKA Manabu: *Senior Scientist, Institute of Observational Research for Global Change, Japan Agency for Marine-Earth Science and Technology*

Water circulation studies using new polarimetric radar

A new polarimetric (multi-parameter) radar was installed at the Hydrospheric Atmospheric Research Center (HyARC), Nagoya University, in 2007. Since installation, this equipment has been promoting new studies on clouds and precipitation, and aiding in the development of new observational and analytical techniques that are essential for studies on water circulation. Such observational and analytical techniques, as well as data assimilation methods, are necessary for the utilization of observational data from the new radar and for amalgamation of the data with a cloud-resolving model.

This research plan aims at promoting new research on water circulation using the new polarimetric radar as well as existing radar sets. In concrete terms, we examine and implement observational data of weather phenomena and physical processes of cloud and precipitation systems. We aim at developing new parameters for multi-parameter radar observation and data analysis and new display methods for radar data. We will develop software and operational routines for the radar from physical and engineering viewpoints in collaboration with researchers participating in this study project.

Diurnal processes of convection/precipitation systems in the climate system

Diurnal variations in convection and precipitation are prominent meteorological phenomena that occur particularly in tropic/subtropic and monsoon regions. Energy, water, and momentum exchanges through the diurnal cycle occur among the Earth's surface, atmospheric boundary layer, and free atmosphere, and play a crucial role in global climate. However, climate models such as a general circulation model (GCM) cannot produce realistic diurnal convection/precipitation cycles, and they continue to exhibit systematic errors.

This research plan aims at clarifying the effects of regionality and seasonality on diurnal processes, based on the Tropical Rainfall Measuring Mission (TRMM) satellite, other remote sensing data, and *in situ* observational data from rain-gauge stations. The plan also uses cloud-resolving models such as CReSS and WRF model as well as other regional models to elucidate systematic errors on the part of climate models in handling diurnal cycles. This work can contribute to the ongoing international project MAHASRI and promote further study of diurnal convection/precipitation cycles in the climate system in Japan.

On March 5-7, 2009, an international MAHASRI/HyARC workshop on Asian monsoons was held in Danang, Vietnam. Studies on diurnal variations in cloud/precipitation systems, taking into account terrain, synoptic conditions, intraseasonal variations, and more, were presented. Ten speakers (including two keynote speakers) presented significant scientific results to over 70 workshop participants.

Global Mapping of Variation in Terrestrial Water Storage

Not much is known about seasonal and climate-related variations in the distribution of terrestrial water. Monthly gravity field estimates made by the twin Gravity Recovery and Climate Experiment (GRACE) satellites have a geoid height accuracy of 2 to 3 mm at a spatial resolution of 400 km. If we could estimate distributions of monthly precipitable water and precipitation, geoid variations could be largely attributed to surface water and groundwater changes. Thus, GRACE observations will help us connect processes at traditional length scales (tens of kilometers or less) to those at regional and global scales. In this research program, we promote GRACE-related research with a focus on global mapping of terrestrial water storage.

HyARC is also conducting mass spectral analyses of stable isotope ratios of water. Stable isotope ratios of water (δD & δ^{18}O) and anomalies from the well-known meteoric water line (d-excess = δD – 8 · δ^{18}O) are good indicators of the origins of precipitation, river water, groundwater, and so on. Because isotope ratios of water are controlled by kinetic or equilibrium fractionation processes in evaporation or condensation, the ratios can be used for evaluating global water cycles as supporting tools for water balance calculation, paleoclimate variation research, and basin-scale hydrological studies. In fiscal 2008, we comprehensively analyzed 2400 water samples upon requests from six domestic researchers.

This research plan also aims to promote studies in terrestrial water storage as well as isotope hydrology, and to link those research activities among several research groups in Japan. We have conducted an annual science workshop related to this research plan. In fiscal 2008, we held a workshop from February 26 to 27, 2009. A total of 37 participants attended the workshop, and valuable discussions were held on the issues described above.

Observational study on atmosphere and ocean over and around the Okinawa Islands

The National Institute of Information and Communication Technology (NICT) established an observation center in Okinawa. Center facilities include a full polarimetric Doppler radar (COBRA), 400-MHz wind profiler radar, Doppler sodar, disdrometers, rain gauges, and ocean radars. Collaboration between NICT Okinawa and HyARC began in 2005, and use of the facility was encouraged as one of the inter-university collaboration activities of HyARC.

During the last three years, the collaborative has produced many study results and have presented in annual project workshops. Study results include better understanding of the following: spatial and temporal variations in the Kuroshio Current around the Okinawa Islands observed by ocean radar; raindrop size distribution characteristics, determined by COBRA polarimetric data; and characteristics of atmospheric low-level jets over Okinawa Main Island, determined by wind profiler data. These study results suggest the possibilities and also the limitations of observations using the NICT Okinawa facility. An advantage is that long-term data have been accumulated, enabling the study of ocean and atmosphere climatology around the Okinawa Islands. A limitation is the observation range of ocean radars is short for the study of spatial variations in the Kuroshio Current around the islands, although synergy with other data such as satellite data mitigates this particular limitation.

In the fiscal year of 2008, this project was restarted under a new Japanese title with a new emphasis on climate. Studies are mainly extensions of previous ones, but new ideas and proposals for the facility have appeared. In addition, the center's infrastructure has been improved, with upgrades to instruments, high-speed communication lines, and more. All of this suggests that the NICT Okinawa facility is now ready to be put to extensive use.

The Innovative Program of Climate Change Projection for the 21st Century (KAKUSHIN Program)

• Cloud Modeling and Typhoon Research

The Innovative Program of Climate Change Projection for the 21st Century (KAKUSHIN Program) is a research program conducted by the Ministry of Education, Culture, Sports, Science, and Technology (MEXT). KAKUSHIN was started in 2007 and will continue for five years. As a part of the program, a research project named "Cloud modeling and typhoon research" is now underway at HyARC (PI: *K. Tsuboki*) to develop a high-resolution cloud-resolving model and to contribute to the accurate projection of future climate by global models. In the second year of the program, our team has been obtaining some research results.

Cloud physics is one of the key processes in modeling studies of climate change, especially studies of global warming. Improvement of the computational scheme of the cloud processes is necessary for accurate simulations in global models. Cloud processes are also core processes in simulations of high-impact weather systems such as heavy rainfalls and typhoons. The following are the four main objectives of the cloud modeling team. (1) Cloud microphysics in the cloud-resolving model Cloud Resolving Storm Simulator (CReSS) will be improved. The dynamic part of the CReSS model will also be improved for accurate and high-speed calculation. (2) Using the CReSS model, cloud parameters of global models will be examined. Satellite observations are used to verify cloud modeling. (3) CReSS is coupled with global models interactively for accurate modeling of convective regions. In particular, convective clouds in the tropical region and typhoons are studied by the modeling system. (4) The CReSS model is also used for typhoon research. The results are used to verifications of typhoon simulations in global models, and to accurate and quantitative evaluations of the impact of typhoons on human society in the present and warming climates.

Regarding the improvement of the microphysical processes of the CReSS model, the process of ice nucleation was examined and improved this year. The sedimentation process of ice particles and the ice-enhancement process were introduced and tested. Without ice enhancement, ice particles are concentrated at the tops of clouds. The enhancement process increases the number concentration just above the melting layer. A large amount of ice was observed just above the melting layer by sounding observations with a hydrometeor-camera. Using the observation data, we verified the results of simulations. To improve the dynamical part of CReSS, we introduced a semi-Lagrangian scheme and made a test simulation of an observed cold front. The scheme increases the integration speed significantly.

This year, we made daily simulation experiments in the regions of the East China Sea and Palau in the tropics with a horizontal resolution of 4 km. Daily simulations with a horizontal resolution of 1 km were also performed in the Tokai and Hokuriku Districts. These experiments produced a large amount of data on clouds and precipitation.

For the evaluation of CReSS to perform a typhoon simulation, we performed a 14-day simulation of Typhoons 16 and 18 of 2004 using the tiling domain technique. The simulated central minimum pressure of Typhoon 18 reached that of the observed typhoon. The simulated rainfall distribution was verified by JMA (the Japan Meteorological Agency) radar-AMeDAS observation. Figure 1 shows that the simulated rainfall distribution around the Kyushu District at 13 days from the initial time is quantitatively similar to the observed rainfall. This indicates that CReSS is useful for typhoon simulations.

The Meteorological Research Institute of JMA simulated the present and global warming climates using a very high-resolution global circulation model (GCM) as part of the KAKUSHIN program. We found very intense typhoons in the model outputs of the GCM and performed cloud-resolving simulations of the typhoons using CReSS. The comparison of the central minimum pressure in GCM and CReSS simulations showed that some typhoons are very much more intense in CReSS than in GCM, whereas others are weak. The correlation of typhoon intensity between GCM and CReSS is very weak. The maximum velocity around the typhoons is usually larger in CReSS than in GCM. In the warming climate simulation, we found super-typhoons, which have an intense maximum sustained wind speed of 67 m/s or greater. No super-typhoon was found in the present climate simulation, suggesting that global warming results in the intensification of typhoons.

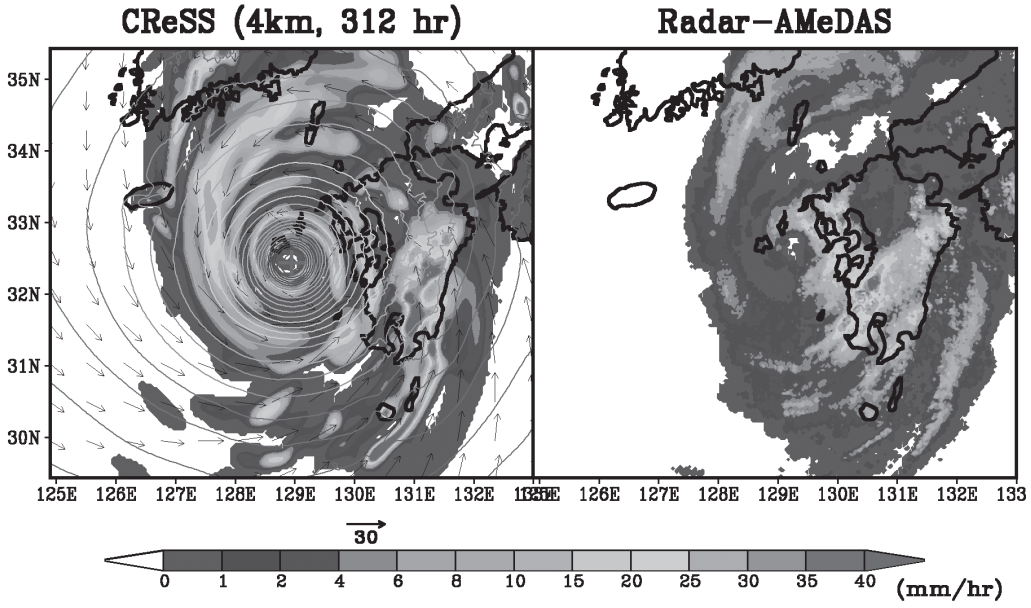

Figure 1. Comparison of rainfall distributions of Typhoon 18 at 13 days from the initial time.
Left panel shows the CreSS simulation using the tiling domain technique; **right panel** shows JMA radar-AMeDAS observations. The center of Typhoon 18 is located west of Nagasaki Prefecture. The contours in the left panel are surface pressure, and the arrows are horizontal wind velocity.

Study consortium for Earth-Life Interactive System (SELIS)

The Study consortiumu for Earth-Life Interactive System (SELIS) was established as a virtual institute in Nagoya University in March 2008, to follow up the research activity of the 21st century COE Program of "the Sun-Earth-Life Interactive System". The member instate of SELIS are HyARC, Graduate School of Environmental Sciences (GSES), Graduate School of Bio-Agricultural Sciences (GSBS) and the Solar-Terrestrial Environmental Laboratory. The SELIS project office is located at the 5th floor of the Institute for Advanced Research Hall of this campus, and the HyARC is managing this office as a main institute of SELIS. The main objective of the SELIS is to promote coopearative studies and relevant capacity building for the Earth-Life Interaction studies, and to promote collaboration with relevant national and international programs and projects. SELIS is also expected to contribute to research projects proposed from Nagoya University to the Research Institute for Humanity and Nature (RIHN) in Kyoto. In the education program, SELIS contributes to some lecture course and seminars, e.g., "Chikyu-gaku" (Study for the Earth) at the GSES.

The kick-off meeting and seminar was held on June 3 2008, and we had eight SELIS seminars in the 2008 school year. In addition, we organized the special lecture in December 1, 2008, on "Current status of global warming research" by Prof. Shukuro Manabe, who is currently a distinguished invited professor. SELIS also organized the 1st SELIS international scientific workshop in January 2009 on "Eco-Climate Dynamics in Monsoon Asia and Eurasia", where five leading scientists for this field were invited from USA, Europe and China.

Solution Oriented Research in Science and Technology (SORST)

• Satellite Monitoring of Ocean Primary Productivity

The ocean is the largest reservoir of water and carbon dioxide on the Earth's surface; hence, the air-sea exchange of water and carbon dioxide plays a central role in determining climate systems on the Earth. The air-sea exchange of heat (water) and carbon dioxide is affected by phytoplankton because they determine the optical properties of the near-surface oceans and absorb carbon dioxide by primary productivity. To better predict climate variability by mechanistic understanding of regulating processes for phytoplankton and improved climate prediction models, global-scale quantitative knowledge of the abundance and productivity of phytoplankton is required. Practically, this knowledge and understanding will be attained only by satellite observations, but because obtaining in situ data for validation of satellite data is difficult, the satellite data have yet to be fully exploited.

To overcome this difficulty, we have been developing a system for in situ monitoring of ocean primary productivity for validation of satellite data. The system, which is composed of an underwater winch system with a profiler buoy equipped with a fast repetition rate fluorometer, was successfully developed with support from Core Research for Evolutional Science and Technology of the Japan Science and Technology Agency (JST). Following this, a continuation project "Satellite Monitoring of Ocean Primary Productivity" (SMOPP) was approved by JST in the Solution Oriented Research in Science and Technology Program in 2004. The goal of the SMOPP project is to design an operational monitoring system for ocean primary productivity on a global scale. To attain this goal, we conduct routine operation of the monitoring system and obtain validated time series satellite data of primary productivity, which will be used in combination with other time series satellite data on physical forcing parameters on the ocean surface, for process studies on the response of ocean biology to atmospheric forcing of the ocean.

Long-term operation of the monitoring system in Sagami Bay has been carried out since 2007 and we were able to operate the monitoring system successfully from November 2007 to November 2008, although it was recovered temporarily for maintenance. As a result, daily vertical profiles of ocean productivity as well as hydrographic parameters, which could not be obtained by ship observations, were derived. To validate the satellite-based process study and reveal temporal and spatial variation in physical and biological phenomena in Sagami Bay, we conducted hydrographic observations four times in the bay. FY 2008 research activities in the SMOPP project are described separately in the activity reports of the Ocean Climate Biology Lab and Bio-physical Oceanography Lab. As for the Primary Productivity Profiler, we continued efforts to conduct as many measurements as possible in various environments such as the northern North Pacific, East China Sea, and Japan Sea. These data are archived in the database after quality control. Since the SMOPP will be completed by next October, we are analyzing huge amounts of data derived under the SMOPP and are finalizing the findings.

Laboratory of Meteorology

Structure of a precipitation system around Aichi Prefecture, Japan on August 28–29, 2008

A precipitation system brought heavy rainfall around Aichi Prefecture on August 28–29, 2008. Total rainfall amounts on these two days were 304.5 mm at Okazaki, 240.0 mm at Ichinomiya, and 202.0 mm at Nagoya. Hourly rainfall amounted to 146.5 mm at Okazaki from 01 to 02 Japan Standard Time (JST) on August 29. In this study, we examine the structure of the precipitation system using a new X-band polarimetric radar situated at Nagoya University and the Cloud Resolving Storm Simulator (CReSS).

From observations using the polarimetric radar, a line-shaped precipitation system aligned from south-southwest to north-northeast propagates southeastward slowly (at about 7 m/s). Southeastern and northwestern regions of the precipitation system in the lower troposphere are occupied by southeasterly and northwesterly winds, respectively; thus, the low-level convergence between these low-level winds should maintain the precipitation system (Fig. 1). The differential reflectivity (Z_{DR}) observed by the polarimetric radar shows the existence of large raindrops whose median volume diameter (D_0) is greater than 2.7 mm. The observation of the ground-based drop size distribution (DSD) using the Disdrometer also shows the existence of large raindrops whose D_0 is greater than 2.3 mm; thus, many large raindrops were formed in the precipitation system and should contribute to the heavy rainfall.

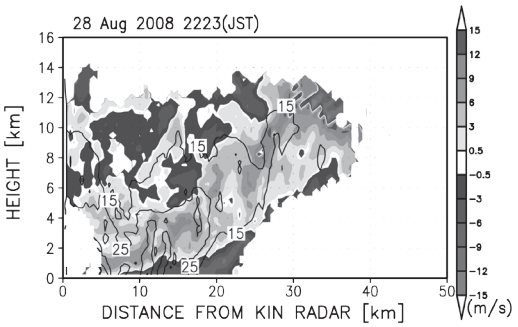

Fig. 1. Vertical cross section of distributions of reflectivity (contour) and Doppler velocity (shades) in the Range Height Indicator (RHI) along the direction of 316.08° from the polarimetric radar situated at Nagoya University at 22:23 JST on August 28, 2008. Light and dark shades show southeasterly wind (away from the radar) and northwesterly wind (approaching the radar), respectively.

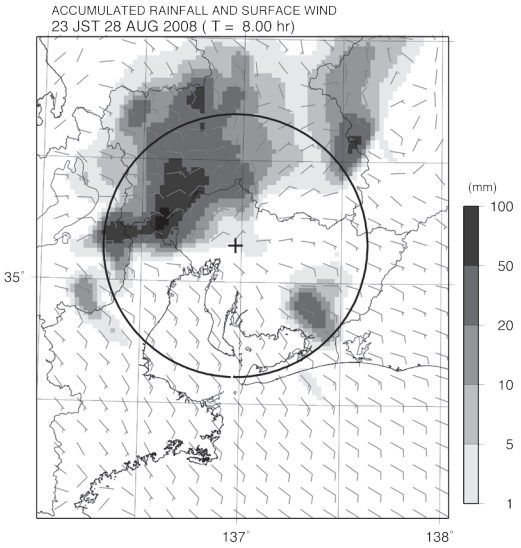

Fig. 2. Simulated horizontal distribution of hourly precipitation amount (mm: shade) from 22:00 to 23:00. Barbs are horizontal wind vectors at the surface at 23:00 JST. Cross and solid circle show the location of the polarimetric radar and observation range (64 km), respectively.

Global Spectral Model (GSM) data provided by the Japan Meteorological Agency (JMA) are used as the initial and boundary conditions of a simulation with a horizontal grid resolution of 2 km using the CReSS. The simulation reproduces well the generation location, propagation direction, and speed of the precipitation system; and the maximum hourly precipitation amount around Aichi Prefecture (Fig. 2). The simulation also reproduces the low-level convergence between the southeasterly and northerly winds below the precipitation system (Fig. 3). The southeasterly is a high equivalent potential temperature (warm and moist) airmass induced by a synoptic-scale situation. On the other hand, the northerly is a relatively low equivalent potential temperature airmass, whose relative humidity is greater than 75%, induced by the downdraft in the precipitation system. Since evaporation cooling is quite limited in a moist environment, the temperature decrease at the surface is only about 2 or 3°C. Although the propagation of the precipitation system shows a gravity-current-like structure by the relatively cool and dry airmass located on the northwestern side of the system, the propagation

speed to the southeastward is slow, because the difference in density of the airmasses between both sides is quite less. The minute effect of evaporation cooling in the precipitation system is the predominant structure under the high humid environment.

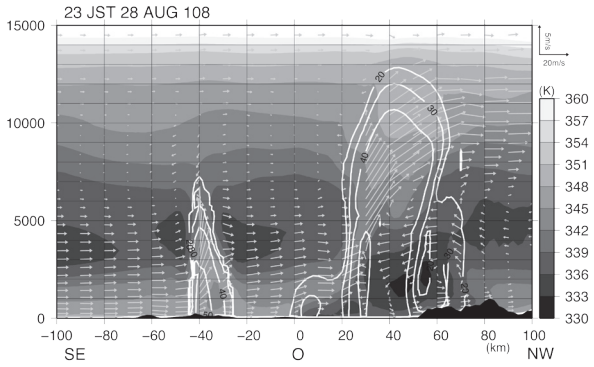

Fig. 3. Simulated vertical cross section of distributions of equivalent potential temperature (shade), estimated reflectivity from mixing ratio of precipitation (rain, snow, and graupel: contour), and wind vectors shown by horizontal wind along the plane and vertical wind (arrows) along the southeast-northwest direction at 23:00 JST. Nagoya University is located at the origin (O).

Formation and maintenance processes of the heavy rainfall event around Fukui Prefecture simulated by the CReSS

A heavy rainfall event was observed around northern Fukui Prefecture on July 18, 2004. The heavy rainfall event is called the Fukui Heavy Rainfall. The event is divided into two stages: the first and second stages are from 01 to 03 and from 05 to 12 JST based on data from the Radar–AMeDAS operated by the JMA. A line-shaped precipitation system is observed initially and changes to an oval-shaped one around 07 JST when the maximum precipitation amount is recorded around Fukui Prefecture.

To reproduce the precipitation system, a simulation with a horizontal grid resolution of 1 km is conducted using the CReSS. The simulation starts at 03 JST on July 18. The simulation reproduces well the distribution and amount of 3-hourly precipitation compared with the Radar–AMeDAS observations (Fig. 4). The maximum precipitation amount, exceeding 50 mm hr^{-1}, around Fukui Prefecture and its time series are also reproduced (Fig. 5). Using the simulation result, the formation and maintenance processes of the precipitation system are examined. Sensitivity tests with modified topography and without evaporation of rain are also conducted to clarify the maintenance process.

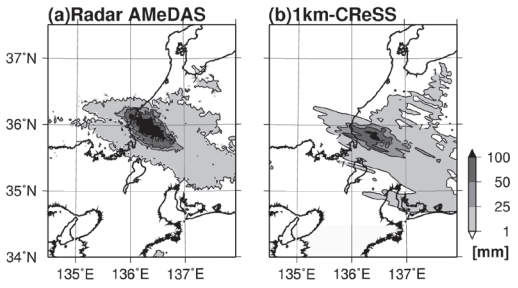

Fig. 4. Horizontal distributions of 3-hourly accumulated rainfall amounts around Fukui Prefecture between 07 and 10 JST of Radar–AMeDAS **(a)** and the simulation **(b)**.

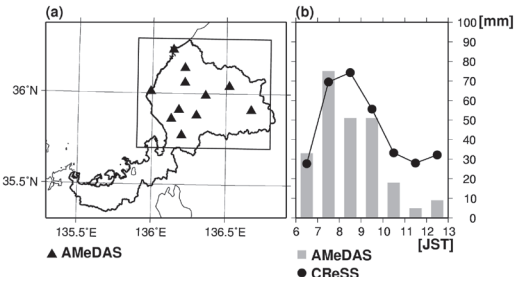

Fig. 5. **(a)** AMeDAS observation sites in northern Fukui Prefecture (▲) and the region in which the maximum hourly rainfall amount is calculated in the simulation result (rectangle). **(b)** Time series of maximum hourly rainfall amount observed by AMeDAS (bar graph) and simulated by the CReSS (solid line) enclosed in the rectangle in (a).

The precipitation system is generated around the Oki Islands where high convective unstable stratification and a weak low-level convergence appear using JMA regional objective analysis (RANAL) data and the simulation result; thus, a convective precipitation system would be easily generated. The system propagates eastward over the Sea of Japan after its generation around there. A westerly wind in the lower troposphere supplies a high equivalent potential temperature airmass that maintains the precipitation system. The system only flows eastward

due to westerly winds in the middle troposphere and does not show the back-building (BB) structure. When the precipitation system reaches Fukui Prefecture, the convergence zone in the lower troposphere is maintained for about one hour. The convergence zone would be maintained by the effects of mountains located along the coastal region of Fukui Prefecture, based on the result of the sensitivity experiment. As a result, new precipitation cells develop over the western tip of the lower convergence zone, i.e., in the upstream (western) side of the pre-existing cells that propagate eastward; thus, this is the BB structure. As the structure of the precipitation system changes to the BB type, precipitation cells intrude continuously over Fukui Prefecture, producing a large amount of rainfall there.

Structure of a developing typhoon simulated by the cloud-resolving model

A warm core and an eyewall cloud are characteristic structures of a typhoon. Numerical simulations using the CReSS with a high horizontal grid resolution are conducted to clarify the structure of the inner region of typhoon T0712. The purpose of this study is to clarify the contribution of the warm core to the development of the typhoon, the origin of the airmass of the warm core, and the structure of the forces that act on the airmass in the inner region of the typhoon.

The simulation reproduces well the track and pressure drop of the typhoon. The typical structures of the typhoon such as the warm core and eyewall clouds, and dynamical characteristics such as low-level inflow, updraft in the eyewall clouds and upper-level outflow in the typhoon, are also simulated successfully. A warm core with a large positive anomaly of potential temperature (greater than 14 K) is generated at a height of about 15 km after 24 h from the initial time (Fig. 6). The positive anomaly of potential temperature contributes to an increase in thickness between 200 and 100 hPa. Although the height of 50 hPa is almost constant with time, the increase in thickness around these levels contributes to the height of 900 hPa; thus, the pressure drops in the lower troposphere around the center of the typhoon.

A back-trajectory analysis is conducted to show the origin of the airmass in the warm core (Fig. 6). The origin of this airmass is divided into two regions. One moves inward in the lower troposphere and ascends in the eyewall clouds, and the other descends from the lower stratosphere. Figure 7 shows time series of potential temperature and equivalent potential temperature of the airmass coming from the lower troposphere. Potential temperature increases greatly between 18 and 20 h after the simulation starts, when the airmass ascends in the eyewall cloud; thus, the airmass should experience diabatic heating. Consequently, one of the origins of the warm core should be diabatic heating in the eyewall clouds.

A forward trajectory analysis is also performed to investigate the dynamical process from the lower troposphere. The analysis shows that most airmass flows outward in the upper troposphere, and only a small amount moves into the warm core. Although the pressure-gradient force mainly acts on the low-level inflow, the centrifugal force is greater than the pressure-gradient force around the inner side of the eyewall in the lower troposphere, where the radial velocity changes from inward to outward. Thus, it produces the low-level convergence below the eyewall clouds and tilts the updrafts in them in the outward direction. This mechanism is common to both outward flow in the upper troposphere and motion into the warm core. Most of the airmass is accelerated outward by the centrifugal force in the upper troposphere; on the

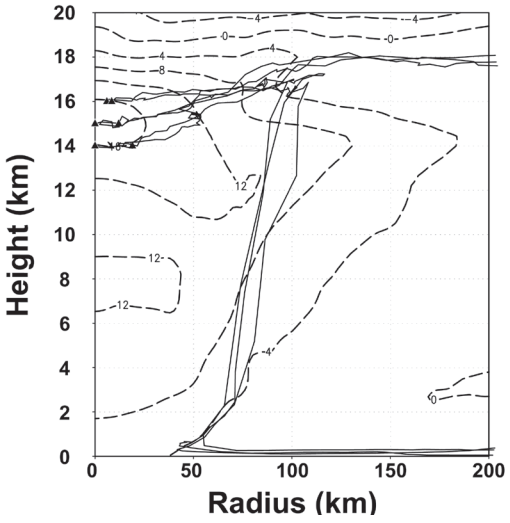

Fig. 6. Radius-height cross section of azimuthally averaged potential temperature anomaly at the center of the simulated typhoon (dashed line) after 24 h from the initial time. Solid lines show parts of the back trajectories. ▲ show the starting points of the back trajectory analysis.

other hand, only a small amount of airmass in which the pressure-gradient force is greater than the centrifugal force drifts into the warm core.

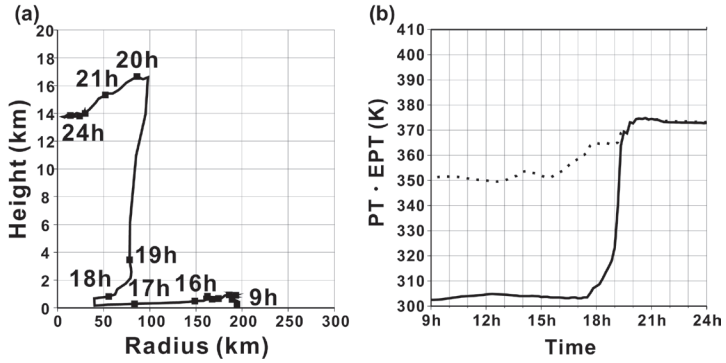

Fig. 7. (a) Radius-height cross section of one back trajectory analysis from the lower troposphere. (b) Time series of potential temperature (solid line) and equivalent potential temperature (dotted line) of the airmass along the trajectory in (a).

Tiling Domain Technique for a Cloud-Resolving Model

The computational domain of most regional models is generally rectangular. However, the region of interest is not always rectangular but is often irregularly shaped. An arbitrary-shaped domain is more suitable for efficient computation of simulations. In the present study, we have developed a new technique to perform parallel computation of a cloud-resolving model in an arbitrary-shaped region, which is named the Tiling Domain Technique (TDT), for the CReSS model.

The arbitrary-shaped domain of parallel computation using the TDT is composed of many small rectangular domains called "domain tiles." If a side of a domain tile is connected to a neighboring domain tile, a halo region is set along the side and data exchange is performed with the neighboring tile by Message-Passing Interface (MPI). If no neighboring domain tile is present, the side is considered a boundary of the computational domain. Each domain tile is further divided into subdomains if necessary. Another parallel computation between subdomains within the domain tile is performed using MPI. The TDT performs these two types of data exchange at different levels. We refer to this type of parallel computation as "hierarchical parallel computations." Multiple computational domains consisting of different numbers of domain tiles in each domain are possible, as well as an isolated domain.

Using the TDT, we perform a simulation experiment of typhoon 0418 (T0418), which caused severe damage all over Japan owing to strong winds. In the experiment, 64 domain tiles are used along the track of T0418, and a one-week simulation is performed. The RANAL data of the JMA are used for initial and boundary conditions. The horizontal grid size is 2000 m, and the experiment is started from the initial conditions of 00 UTC September 1, 2004. The central pressure of the simulated typhoon decreases rapidly and reaches that of the best-track data after about 3 days from the initial time. The simulated typhoon almost follows the JMA best track for the 7 days of the simulation period. Figure 8 shows the comparison of simulations of the T0418 using the TDT and all domain at the 6 days from the initial time. The TDT result of the distribution of precipitation amount corresponds to that using the all domain. The corners of the TDT result do not affect the simulation result compared with that using the all domain. When the simulated typhoon approaches western

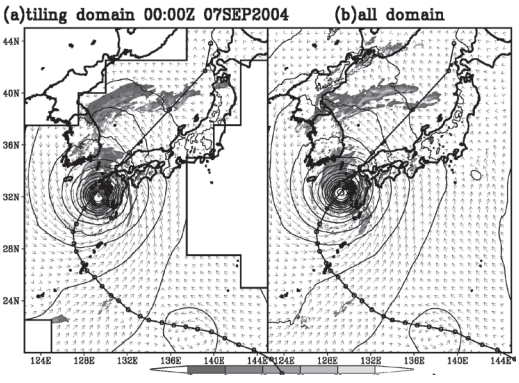

Fig. 8. Comparison of simulations of the typhoon 0418 in September 2004 using the tiling domain technique (a) and all domain (b) at 6 days (518400 seconds) from the initial time. The gray levels are precipitation intensity (mm/h) and contour lines are sea-level pressure. The arrows are horizontal wind vector at the surface. The solid line is the best track of the typhoon 0418 provided by the JMA.

Japan, it causes heavy rainfall over the land. The distribution and intensity of the simulated rainfall correspond well to the observed rainfall.

Because a typhoon moves along a long curved track, the TDT is an efficient method for high-resolution simulation of the typhoon. Domain tiles are set along the typhoon track, and total computational cost is reduced. The TDT increases the flexibility and applicability of the cloud-resolving model for many different types of weather systems. For example, a computational domain is set along the Japanese Islands, and isolated domain titles are set in the region of individual islands. Another possible application is convective activity in the tropical regions, where the nonhydrostatic effect is crucial. A nested simulation in global circulation model (GCM) using the TDT will be also useful for dynamical downscaling of typhoons.

Development of a three-dimensional detection algorithm for precipitation cells in East Asia during the Meiyu/Baiu period

A precipitation cell is a fundamental element of precipitation systems. To clarify the general features of precipitation cells, statistical analyses are needed. In this study, a three-dimensional detection algorithm for precipitation cells has been developed. Figure 9 shows the definition of precipitation cells using reflectivity data. The central parts of the precipitation cells are recognized by connecting negative regions of the second derivative for three-dimensional reflectivity data. After connecting the central parts of precipitation cells vertically, the three-dimensional region of each cell is fixed.

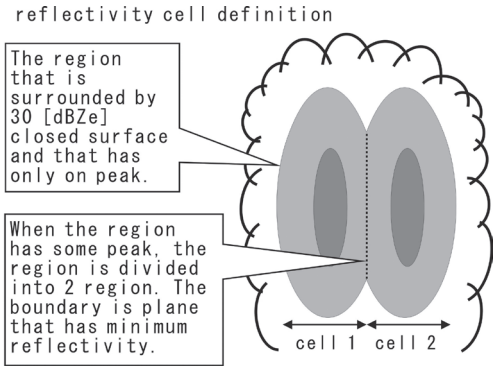

Fig. 9. Definition of precipitation cells using reflectivity data.

The 811 precipitation cells obtained by Doppler radar in three observation projects conducted in East Asia during the Meiyu/Baiu period are detected by human eyes to validate the algorithm. More than 98% of precipitation cells are detected using the algorithm on the same observation data. Thus, the algorithm would have sufficient accuracy and would be reliable for statistical analyses of precipitation cells.

The algorithm can also detect "updraft cells" and "downdraft cells" to apply three-dimensional wind field data calculated from dual-Doppler analyses. Matching up the precipitation cells with updraft and downdraft cells marks the developing, mature, and decaying stages in their life-cycle. Figure 10 shows a schematic illustration of discriminating the stages of precipitation cells. To verify the discrimination, two precipitation cells that were observed in the dual-Doppler region through almost all of their life-cycle are chased, and stages in their life-cycle are discriminated based on wind fields by human eyes. The algorithm's results are consistent with those from human eyes.

The discrimination of stages is conducted using dual-Doppler analyses around Miyako Island (the Southwest Islands of Japan) during the Baiu period in 2006. Precipitation cells in the developing, mature, and decaying stages are detected

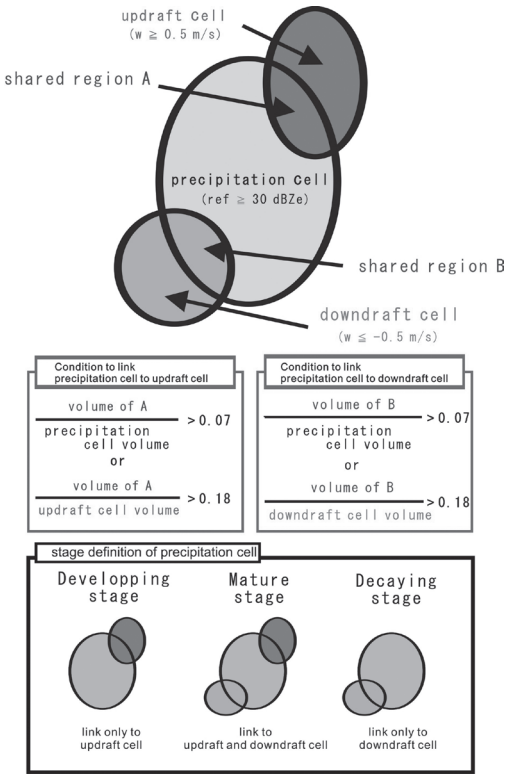

Fig. 10. Schematic illustration of discriminating the stages of precipitation cells.

(183, 154, and 124, respectively). The volume of precipitation cells in the mature stage is greater than at other stages. Although the echo top height of precipitation cells in each stage is almost constant through their life-cycle, the area of precipitation cells in the mature stage is almost twice that at other stages. As a result, the volume of precipitation cells in each stage should depend on their area.

Development of a cumulus boundary layer over land

Development of a cumulus boundary layer over land is investigated using idealized high-resolution numerical simulations with the focus on the onset of "active cumulus" and the effect of external factors: initial amount of water vapor, static stability, and surface energy partition.

A simulation with a horizontal grid resolution of 100 m is conducted using the CReSS. The parameters of idealized initial profile and land surface are set using observational data obtained in the Huaihe River Basin in China on June 20, 2004. Land surface is set to water paddy fields, which are characterized by large latent and small sensible heat fluxes. In the control experiment, the cumulus boundary layer experiences transition from a condition in which only forced cumulus exists (forced cumulus boundary layer) to a condition in which active cumulus also exist (active cumulus boundary layer) at about 1220 local standard time (LST). The active cumulus onset is almost coincident with an abrupt drop in the level of free convection (LFC: Fig. 11). The LFC drop is attributed to a decrease in the local minimum value of saturated equivalent potential temperature at the bottom height of the inversion layer, in addition to an increase of equivalent potential temperature near the land surface (Fig. 12). After the active cumulus onset, the inversion height maintains a large rate of increase because evaporation of cloud water cools and moistens the inversion layer.

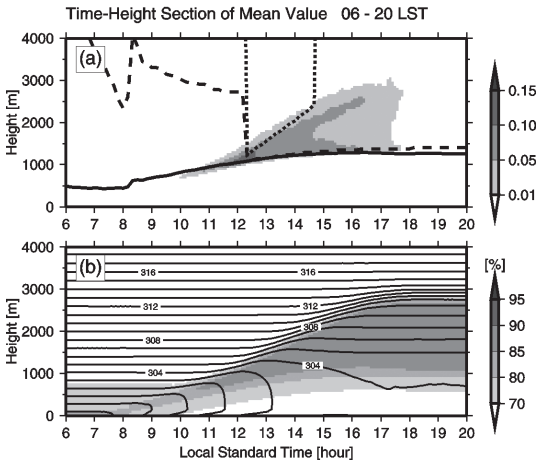

Fig. 11. (a) Time-height cross section of cloud fraction (shade) and time series of lifting condensation level (LCL: solid line), LFC (broken line), and level of neutral buoyancy (LNB: dotted line) calculated from mean values at a height of 45 m (lowest level of model domain). **(b)** Same as (a) but for mean relative humidity (shade) with mean virtual potential temperature (contours, every 1 K).

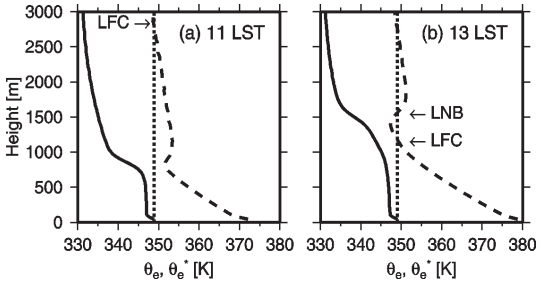

Fig. 12. Profiles of mean equivalent potential temperature (solid lines) and saturated equivalent potential temperature (broken lines) at 11 LST (a) and 13 LST (b). Dotted lines indicate the mean equivalent potential temperature of air near the land surface (at a height of 45 m).

Systematic sensitivity experiments show that the onset time arrives earlier with greater initial water vapor, smaller static stability, and greater evaporative efficiency through changes in the time tendency of saturated equivalent potential temperature at the bottom height of the inversion layer and equivalent potential temperature near the land surface. Since the development of the active cumulus boundary layer causes a large rate of increase of the inversion height, an earlier active cumulus onset leads to a higher inversion height. As a result, water vapor does not accumulate in the lower troposphere and is transported up to the inversion layer; thus, it contributes to the development of a deep moist layer. Therefore, this study demonstrates the interaction between features of the atmospheric environment, such as initial water vapor profile and static stability, and shallow cumulus clouds.

Laboratory for Climate System Study

Intraseasonal Variability of the East Asian Summer Monsoon

The mei-yu–baiu front is an important cloud and precipitation system of the East Asian monsoon, providing large amounts of precipitation in early summer (Fig. 1). The front forms as a subtropical front under the influence of atmospheric circulation in the midlatitudes and subtropical/tropical monsoon regions. The mei-yu front includes both tropical and extratropical variations because of its geographical location. Therefore, tropical and extratropical interactions are an inherent property of the variation. During boreal summer, midlatitude systems that vary on submonthly (7–25 days) time scales favorably propagate along the Asian westerly jet. Thus, a close relationship between midlatitude systems and mei-yu variability in early summer could be expected. Based on submonthly convective fluctuations over the Yangtze and Huaihe river basins (YHRBs) during the mei-yu season (June 10–July 10), we examined the spatiotemporal evolution of convection and circulation over East Asia, focusing on the relationship between upper-level atmospheric circulation in the midlatitudes and convection over the YHRBs. Data used in this study are outgoing longwave radiation (OLR) and National Centers for Environmental Prediction/ National Center for Atmospheric Research reanalysis data for the period between 1979 and 2004. 7- to 25-day filtered OLR anomalies averaged over the key region (25–35°N, 110–120°E) were used as indices to study submonthly variation over the YHRBs.

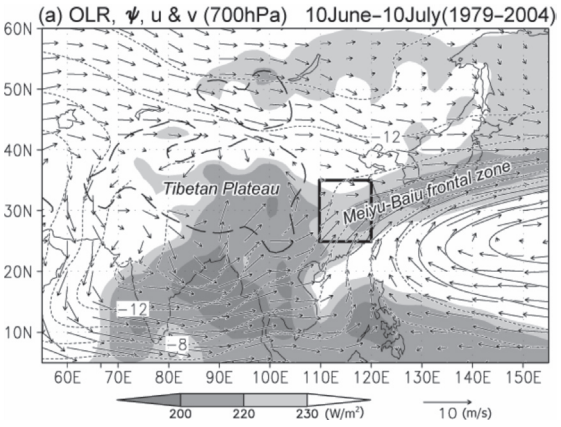

Fig. 1: Mean OLR (shading), 700-hPa stream function, and wind vectors for the mei-yu period (June 10–July 10; 1979–2004). The topographic contour line for 1500 m is also shown (thick dashed line). The key convective variation region is enclosed by the 25–35°N, 110–120°E grid box.

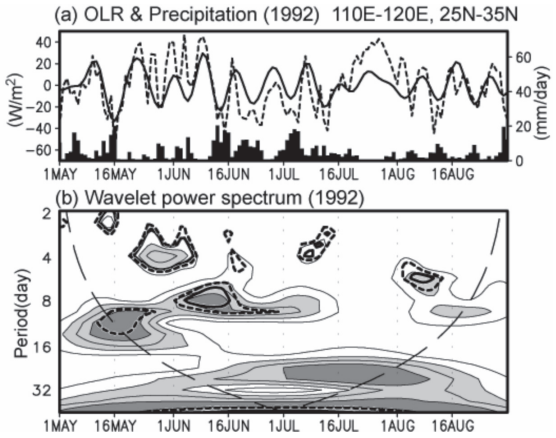

Fig. 2: (a) Time series of detrended OLR anomalies (dashed line), 7- to 25-day filtered anomalies (solid line), and unfiltered precipitation (black bar) averaged over the key region for 1992. (b) The local wavelet spectrum of the detrended 1992 OLR anomalies. The thick solid (dotted) contour line encloses regions of 95% (90%) confidence for a red noise process with a lag-1 coefficient.

7- to 25-day OLR variance averaged over the key region shows large interannual variation over the key region during the mei-yu period. We scrutinized active submonthly intraseasonal oscillation (SISO) years (12 years: 1981, 1985, 1986, 1989, 1992, 1993, 1995, 2000, 2001, 2002, 2003, and 2004). In years of suppressed SISO, we found ISOs of approximately 30 days (e.g., 1988, 1991, 1994, and 1998) and less remarkable ISOs of both submonthly and longer

time scales (e.g., 1980, 1983, 1987, and 1996). Figure 2 shows time series of OLR anomalies and precipitation in 1992. The 1992 OLR anomalies have quasi-periodic oscillation with three active convection phases during the mei-yu period (Fig. 2a). The active phases include heavy and continuous precipitation (10–20 mm/day). The wavelet spectrum shows a statistically significant peak with a period of approximately 7–12 days during the mei-yu period (Fig. 2b). Remarkable submonthly-scale ISOs can be observed during the mei-yu period in the other years analyzed.

To examine the relationship between convection over the YHRBs and upper-level atmospheric circulation, correlation coefficients between OLR anomalies over the key region and 200-hPa streamfunction anomalies in each grid in the 7- to 25-day bands are shown in Fig. 3. Correlation distribution shows two contrasting patterns, suggesting that the dominant processes inducing SISO in mei-yu activity are different, even though they have the same submonthly time scales. Figure 3a shows that large values extend from the northern to eastern peripheries of the Tibetan Plateau (hereafter defined as the NET pattern). Active (suppressed) convections over the YHRBs are associated with an anomalous trough (ridge) to the north of the YHRBs and an anomalous ridge (trough) to the south of the YHRBs in the upper troposphere. In contrast, in Fig. 3b, high correlation coefficients appear along approximately 30°N across the Tibetan Plateau with a wave-train-like distribution (hereafter defined as the AT pattern); the entire key region has negative correlations. Active (suppressed) convections over the YHRBs are associated with the upper-level anomalous ridge (trough).

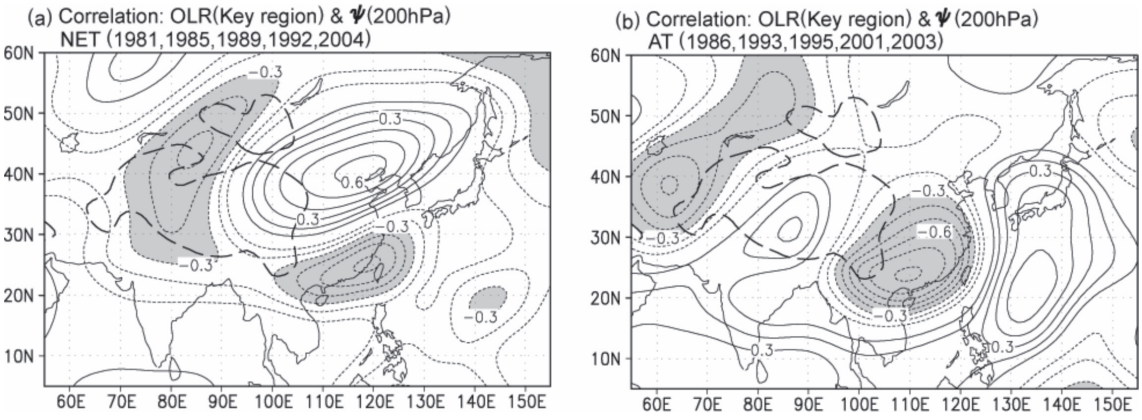

Fig. 3: (a) Correlation coefficients between 7- to 25-day filtered OLR anomalies over the key region and 200-hPa stream function anomalies in every grid in the 7- to 25-day bands for 1981, 1985, 1989, 1992, and 2004. The contour interval is 0.1. (b) As in (a), but for 1986, 1993, 1995, 2001, and 2003.

Composite analysis of the NET pattern shows slow southward migration of convection anomalies from the northeastern periphery of the Tibetan Plateau to southern China, in relation to southward migration of the mei-yu front caused by simultaneous amplification of upper- and low-level waves north of the YHRBs. In the AT pattern, convection anomalies migrate eastward from the western Tibetan Plateau to the YHRBs. A low-level vortex is created at the lee of the plateau by eastward moving upper-level wave packets and associated convection from the plateau.

Rossby wave trains along the Asian jet characterize upper-level circulation anomalies in the two patterns. Basic state of the Asian jet during the mei-yu season differs between the two patterns, especially around the Tibetan Plateau. The Asian jet has a northward arc-like structure in NET years, whereas a zonal jet dominates in AT years. These differences could alter the Rossby wave-train propagation route. Furthermore, AT waves have a larger zonal wave-

number (approximately 7–8) than NET waves (approximately 6), indicating a faster zonal phase speed relative to the ground in the AT pattern than in the NET pattern. These differences likely explain meridional amplification of waves north of the YHRBs in the NET pattern and eastward wave movement across the plateau in the AT pattern. (Fujinami and Yasunari 2009, Mon. Wea. Rev.)

Mechanism of the decreasing trend of monsoon rainfall in September over the Indochina Peninsula

We examined the decreasing trend in rainfall during the late summer monsoon season (September) in Thailand from 1951 to 2000 and associated changes in tropical cyclone (TC) activity. Thailand receives significant rainfall from May to October and experiences 2 rainy peaks in late May to early June and in September. A previous study reported a decreasing trend in September rainfall in Thailand and, based on a regional climate model, suggested that this trend was associated with local deforestation. However, the long-term trend may also be affected by changes in large-scale circulation. Thus, we investigated changes in large-scale circulation associated with the decreasing rainfall trend.

Westward-propagating TCs from the South China Sea and the western North Pacific brought most of the rainfall over Thailand in September. TCs include tropical depressions, tropical storms, severe tropical storms, typhoons, and residual lows. Furthermore, 70% of September rainfall was estimated to be associated with TCs. The 50-year time series of September rainfall over Thailand showed a significant decreasing trend. TC activity, defined by 700-hPa relative vorticity, showed a weakening trend over the Indochina Peninsula (Fig. 4).

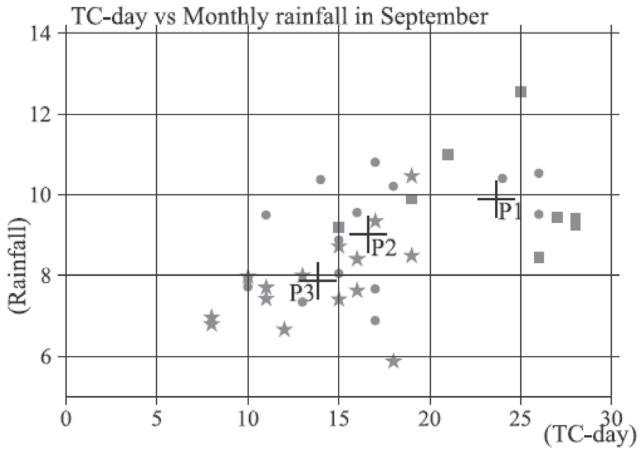

Fig. 4: Scatterplot of September rainfall over Thailand and TC days defined by 700-hPa relative vorticity. Rectangle, circle, and star symbols indicate the relationship in each year during P1, P2, and P3, respectively. The crosses labeled P1, P2, and P3 show the mean relationship of each period. There were fewer samples for P1 than for the other 2 periods because of limitations of the ERA-40 dataset.

TC tracks also suggested weakening TC activity over this area (Fig. 5). The long-term trend in rainfall during the late summer monsoon season was closely associated with changes in TC activity over the Indochina Peninsula; these changes were probably caused by changes in the major course of TCs. Concurrent with the changes in TC tracks, a change in the TC steering current occurred around the Philippine archipelago and Taiwan. This led to the TC activity over the Indochina Peninsula being inactive, probably resulting in the long-term decrease

in rainfall over Thailand. (Takahashi and Yasunari, 2008, JMSJ)

To address the mechanism for the decrease in rainfall, we performed long-term simulations and discussed the effects of long-term changes in both local surface conditions and large-scale circulation. Long-term high-resolution simulation accurately captured the climatological rainfall distribution and quantity. A 30-year run simulated the interannual variation and long-term change in rainfall, both of which were in close agreement with observations (Fig. 6). Spatial distribution of the long-term change in rainfall was also found to be in close agreement with observations. A long-term decrease in rainfall was observed along the major route of westward-moving TCs, including the eastern coast of northern Vietnam, rather than just over Thailand. Finally, the simulated monsoon trough weakened from T1 to T2, which again was consistent with observations. All these long-term changes in rainfall were realistically simulated without including the effects of deforestation in the model. The effects of deforestation over the Indochina Peninsula in September were probably spatially limited, and hence, are not likely to explain the observed decrease in rainfall. Weakening of TC activity over and around the Indochina Peninsula could explain the spatial distribution of the observed decrease in rainfall. Therefore, we conclude that the observed long-term decrease in September rainfall was caused by the change in TC activity, rather than by changes in local surface conditions. (Takahashi et al. 2008, ASL)

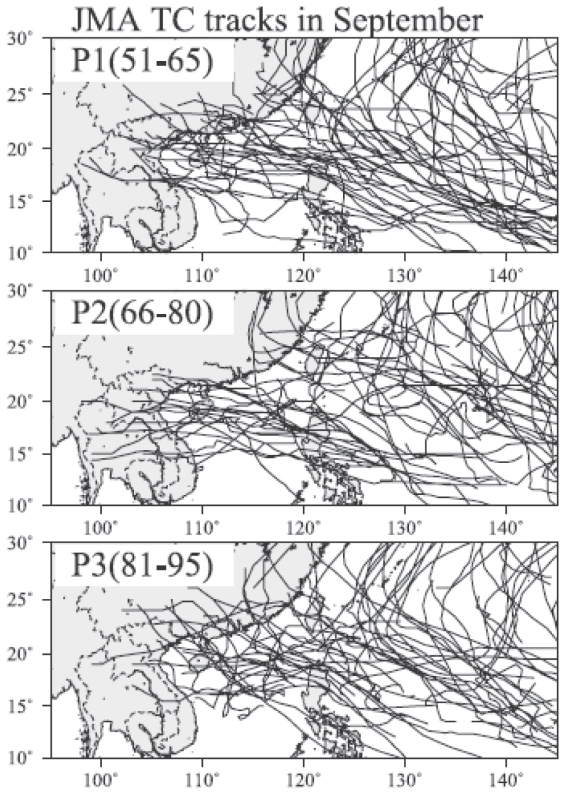

Fig. 5: Japan Meteorological Agency (JMA) TC tracks in September during P1, P2, and P3. Some tracks start from the midstream of a TC lifetime, whereas other tracks end in the midstream. Only TC tracks in September were plotted. JMA TC tracks do not include TCs weaker than a tropical storm.

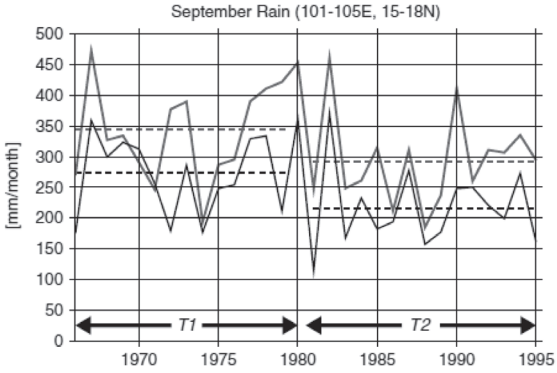

Fig. 6: Time series of the observed September rainfall 10-point average (black) and the simulated September rainfall domain average (gray). The 10 stations were located within an area at 101–105°E, 15–18°N. Simulated rainfall was domain-averaged within the box. The units of rainfall are mm per month. The gray (black) dashed lines denote 15-year averages of simulated (observed) rainfall for each term.

Loboratory for Cloud and Precipitation Climatology

The southeastern Pacific warm band and double intertropical convergence zones (ITCZ)

The intertropical convergence zone (ITCZ) over the east Pacific Ocean remains 5–10° in latitude north of the equator most of the year. However, a southern-hemisphere branch of the ITCZ also often emerges from March to April in the east Pacific, resulting in a double ITCZ. We have no satisfactory explanation to date as to what promotes the double ITCZ in austral fall and hampers it in boreal fall. This study is aimed at determining the growth mechanism of the east Pacific double ITCZ in austral fall.

Satellite measurements from the Tropical Rainfall Measuring Mission (TRMM) and QuikSCAT are analyzed to derive 8-year climatologies of sea surface temperature (SST), surface convergence, column water vapor (CWV), shallow and deep precipitating clouds, and surface heat fluxes from 2000 to 2007. SST produces the initial signature of the south ITCZ, referred to as the southeast Pacific warm band, as early as January. A pronounced feature of the warm band is a local SST maximum around 90°W, resulting from the sum of different surface heat fluxes having different signs and competing geographical patterns. Surface convergence and CWV gradually develop along the southeast Pacific warm band. The population of shallow cumulus starts growing to form the south ITCZ in February, a month earlier than vigorous deep convection that finally organizes in the south ITCZ in March. The double ITCZ therefore does not emerge abruptly in austral fall, but results from a series of distinctive evolutionary stages in the preceding months, initiated by SST in the preceding austral summer.

Simple experiments are next performed to diagnose the key factors that give rise to the southeast Pacific warm band. In the experiments, the heat budget of the ocean mixed layer is calculated with the surface heat fluxes (longwave, shortwave, latent heat, advection, and upwelling), all derived from satellite observations. The results suggest that the absorbed shortwave flux primarily drives the southeast Pacific warm band, enhanced to a lesser extent by ocean upwelling (Figure 1). Insolation remains near the annual maximum from austral summer through late February over the latitudinal range of the south ITCZ, resulting in a peak in tropical southeast Pacific SST and the south ITCZ in March. It is now obvious why the double ITCZ is absent in boreal fall: the incoming shortwave flux is at a minimum in the preceding solstice season and thus incapable of maintaining a warm ocean surface in the southern hemisphere. The ocean mixed layer tends to cool in July, when the shortwave flux is overwhelmed by negative fluxes such as latent heat and longwave fluxes.

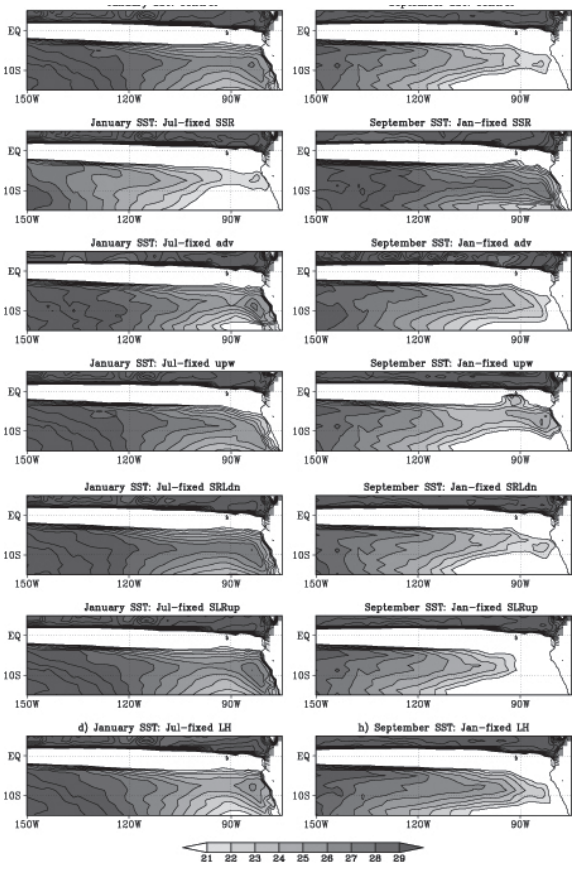

Fig. 1: SST computed from different experiments. **(Left)** January-mean SST with a July-fixed flux. **(Right)** September-mean SST with a January-fixed flux. **(From top to bottom)** control, shortwave-fixed, advection-fixed, upwelling-fixed, longwave ↓-fixed, longwave ↑-fixed, and latent heat-fixed runs.

Variability of cirrus clouds over the Indian Ocean in boreal summer

A primary source of tropical cirrus clouds is often considered to be detrainment from deep convective clouds. In general, the global distribution of cirrus clouds closely resembles the spatial pattern of deep convection in the tropics. This is, however, not always the case. Figure 2 shows that cirrus clouds in boreal summer are spread across the entire Indian Ocean, while deep convective clouds are confined to the eastern part of the ocean and the Bay of Bengal. Cirrus clouds over the equatorial Indian Ocean do not accompany deep convection, implying that a mechanism other than detrainment is at work for the formation and maintenance of cirrus clouds in this particular example.

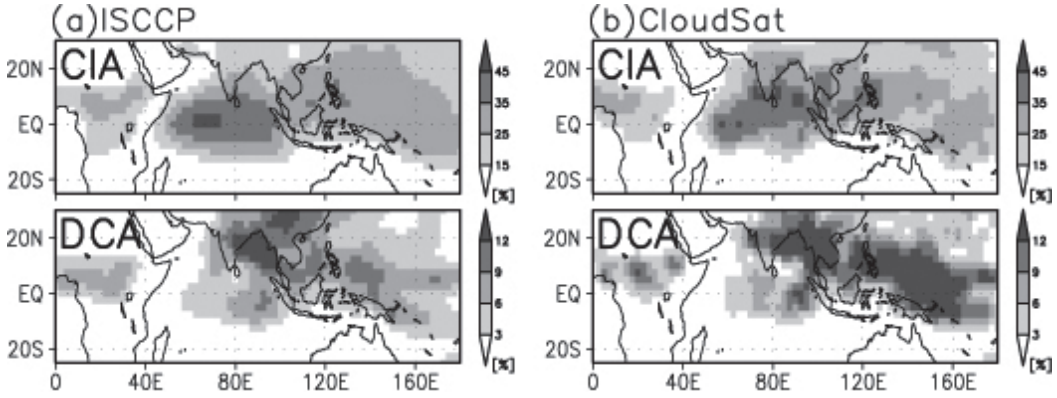

Fig. 2: Climatological boreal summer (June–August) of (top) cirrus cloud amount (CIA) and (bottom) deep convective cloud amount (DCA): **(a)** From the ISCCP product for 1998–2005; **(b)** from the Cloud Sat product for 2006.

To explore this problem, temporal and spatial variations of cirrus clouds over the equatorial Indian Ocean are analyzed using the International Satellite Cloud Climatology Project (ISCCP) cloud datasets. Figure 3 shows the temporal variations of cirrus cloud amount (CIA) and deep convective cloud amount (DCA) over the equatorial Indian Ocean for 1998–2005. CIA is not always in phase with DCA, having pronounced maxima that often do not accompany DCA peaks. Figure 3 also shows a 150-hPa temperature anomaly and 150–300-hPa zonal wind shear. CIA varies in parallel with temperature anomaly and vertical wind shear from time to time. It is suggested that fluctuations in upper-tropospheric temperature and/or wind shear play some role in the in-situ formation of cirrus clouds without detrainment from deep convection.

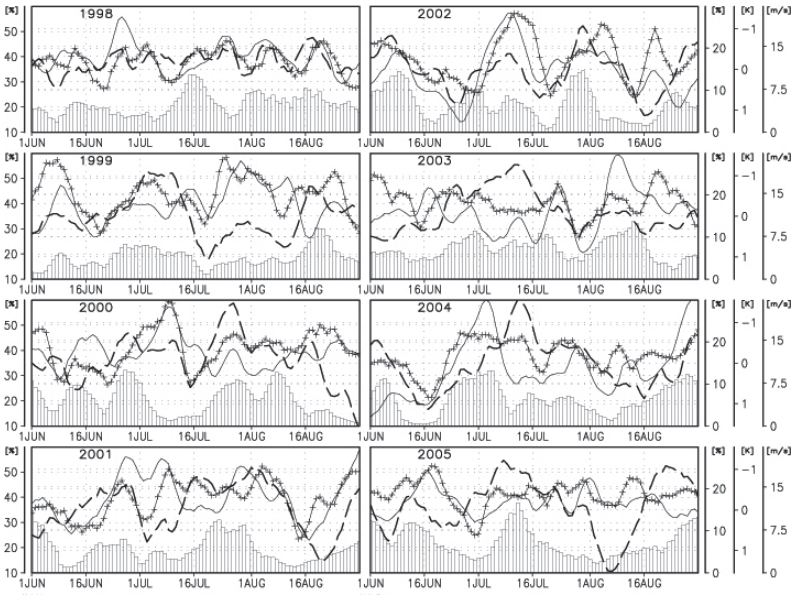

Fig. 3: Time series of CIA (line with crosses), DCA (histogram), 150-hPa temperature anomaly (dashed line), and vertical wind shear between 150 and 300 hPa (solid line) for 1998–2005.

Loboratory of Satellite Meteorology

Diurnal Variations in Low-Level Jet around Okinawa Island, Japan during Baiu Season

Horizontal winds with high temporal and vertical resolution from the 400-MHz wind profiler radar (WPR) at Okinawa, Japan and the Japan Meteorological Agency (JMA) WPRs at three stations surrounding Okinawa were used to investigate the low-level jet (LLJ) during the Baiu season months (May–June of 2004–2006), over the southwest islands of Japan. To better understand the relationship of the LLJ to the Baiu rainfall system, the diurnal variations in precipitation associated with the Baiu front over this region were examined using GSMaP (Global Satellite Mapping Precipitation) and Radar-AMeDAS (Automated Meteorological Data Acquisition System) rainfall data.

First, LLJ characteristics were investigated in two subperiods: the Baiu season over Okinawa Island and the post-Baiu season when the Baiu front has moved further north of Okinawa. LLJ occurrence varies diurnally with a maximum in the night-time and early morning, especially in post-Baiu season. Upper-air soundings suggest that the preference for nocturnal occurrence arises from the reduction of vertical mixing in the atmospheric boundary layer after sunset. Data from the JMA WPR network for three other stations surrounding Okinawa Island show more evidence for the role of the atmospheric boundary layer in generating diurnal variations in LLJ occurrence.

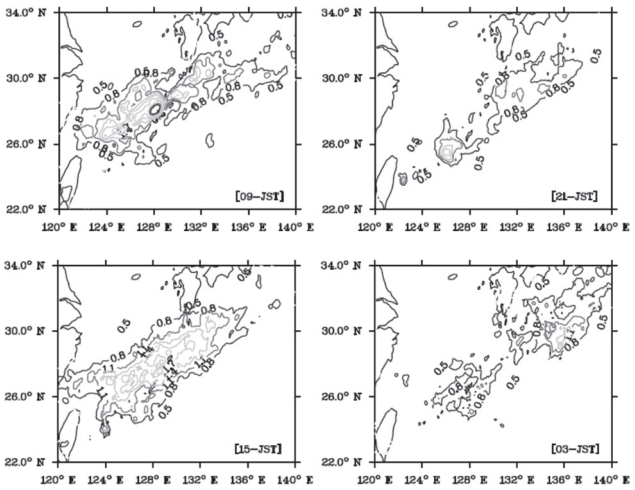

Fig. 1. Diurnal variations in precipitation distribution around Okinawa Island for May and June in 2004–2006, obtained from a satellite rain map.

Therefore, diurnal variations in LLJ occurrence were analyzed with focus on the rain cases. Baiu precipitation over the studied region varies diurnally, with peak intensity in the morning and propagation from northwest to southeast. Thus, peak LLJ intensity in the morning at Okinawa is associated with propagation of a strong precipitation band toward Okinawa Island. However, the preferences for night-time occurrence at Naze and Yonaguni were likely related to the closeness of precipitation when it approached those sites. Yakushima shows less clear diurnal variations in both LLJ occurrence and precipitation.

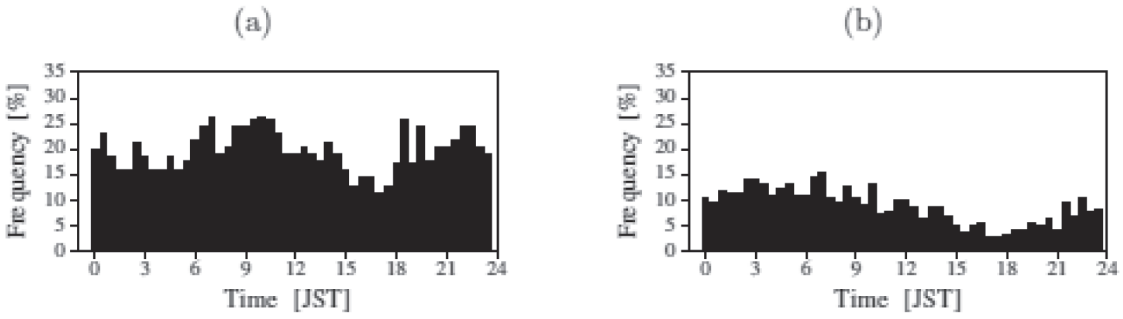

Fig. 2. Diurnal variations in low-level jet occurrence over Okinawa Island for May and June in 2004–2006: **(a)** Rain cases; **(b)** No-rain cases.

Precipitation Characteristics over the Tibetan Plateau in Monsoon Season

The diurnal cycle of rainfall over the Tibetan Plateau is investigated by examining data acquired by the Tropical Rainfall Measuring Mission (TRMM) Precipitation Radar (PR) over June–August of 1998–2007. High spatial resolution data (0.05° × 0.05° grid: ~5 km × 5 km) were used to identify topographic features over the complex region of the plateau. Diurnal variations in rainfall amount, rainfall frequency, rain-conditioned rain rate, and storm height were analyzed to determine the characteristics of precipitation. Distinct diurnal variations were seen over hilly regions, valleys, and 13 large- and -medium sized lakes.

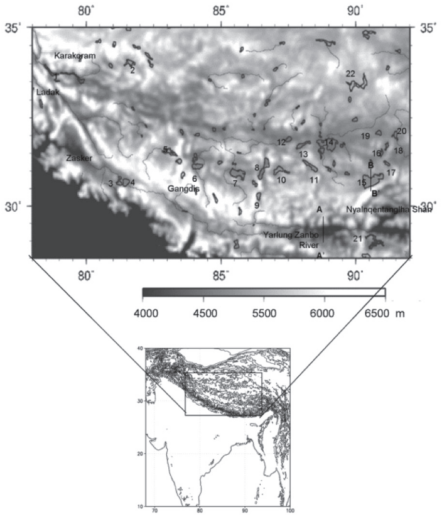

Fig. 3. Topography of the Tibetan Plateau.

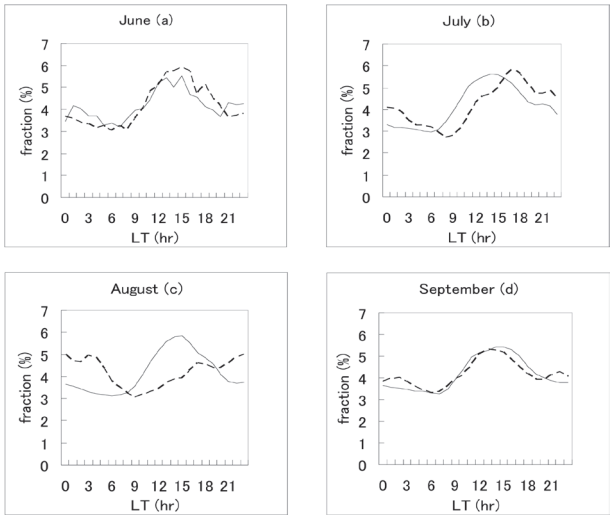

Fig. 4. Diurnal variations in rainfall frequency (broken line) and rain-conditioned rain rate (solid line) in fraction in June for the years 1998–2007; the abscissa is the local time (LT) in hours and the ordinate is the rain fraction in percentage: **(a)** June; **(b)** July; **(c)** August; **(d)** September.

The Tibetan Plateau receives 300 mm of rainfall per year with more than 70% of rainfall in June–August. Of these, July shows the strongest diurnal variation during summer. In July, the peak time of convective rain is followed by the peak frequency of rainfall. Nocturnal and early-morning rainfall shows a mixture of convective and persistent rainfall. In summer, precipitation activity over the Tibetan Plateau is generally strongest during late afternoon. Hilly regions show dominant afternoon/late-afternoon peaks, while valleys show dominant late-evening and morning peaks. Similarly, lakes show late-evening and morning peaks. Valleys with high surface undulation also show strong diurnal variation. Morning rainfall is distinctly evident over lakes. Peak rainfall time over lakes depends on lake size and topographic slope around the lake. On average, the strength of the diurnal variation over a lake varies inversely with the lake size. In this region air is rather dry and has weak prevailing winds. Slope alone is insufficient, but a combination of lake water and surrounding slope may enhance morning rain.

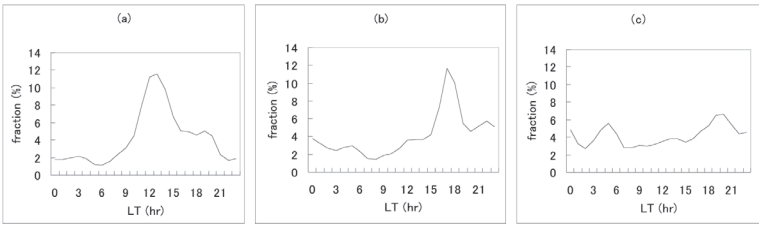

Fig. 5. Diurnal variations in rainfall for 1998–2007; the abscissa is the local time (LT) in hours and the ordinate is the rain fraction in percentage: **(a)** Over the northeastern hilly region of study [33.5°–34.5°N, 91°–92°E]; **(b)** Yarlung Zanbo river valley; **(c)** Lake 15 in Fig. 3.

Laboratory of Eco-Hydrometeorology

Day-to-day variation in diurnal maximum height of the atmospheric boundary layer over the Loess Plateau in China

Temporal variations in the atmospheric boundary layer (ABL) over the Loess Plateau are examined with a focus on day-to-day variations in the diurnal maximum ABL height. The half-hourly ABL height was determined from vertical profiles of turbulence intensity observed by a wind profiler radar. On days with extensive cloud cover by stratiform clouds, the ABL was poorly defined, and estimating its height was not feasible. Accordingly, the ABL height was estimated only for clear or partly clear days, which were selected with the use of net longwave and downward shortwave radiation observed at the surface (Fig. 1). The maximum ABL height varied significantly from day to day. In the afternoon on clear days, cumulus clouds formed frequently and a deep cumulus-topped boundary layer developed. The diurnal maximum ABL height (Z_i) reached as high as 3 km above the surface, which was much higher than that estimated using a slab model (Z_{ical}) with surface heat fluxes (Fig. 2). When the ABL grew to high altitudes and was topped by cumulus clouds, the vertical gradient of potential temperature was relatively small above the ABL top (Fig. 2). This observation suggests that atmospheric stability above the capping inversion was sufficiently weak to allow cumulus cloud formation. Thus, the diurnal maximum ABL height over the Loess Plateau depends on not only surface heat fluxes but also the atmospheric stability above the capping inversion.

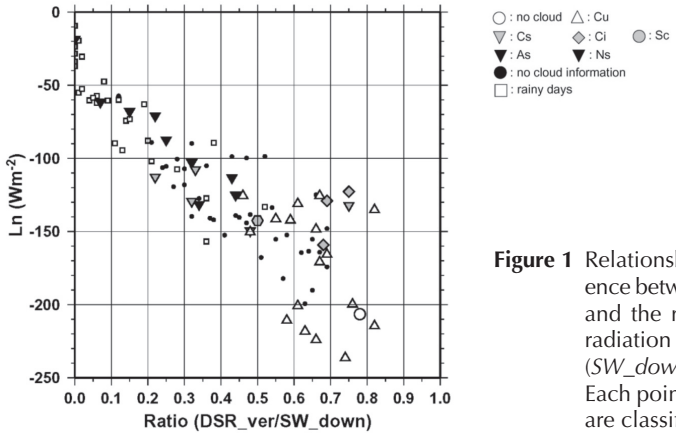

Figure 1 Relationship between net longwave radiation (*Ln:* difference between downward and upward longwave radiation) and the ratio of the vertical component of direct solar radiation (*DSR_ver*) to downward shortwave radiation (*SW_down*) from April to July 2005.
Each point indicates the daytime average value. The plots are classified based on the cloud type.

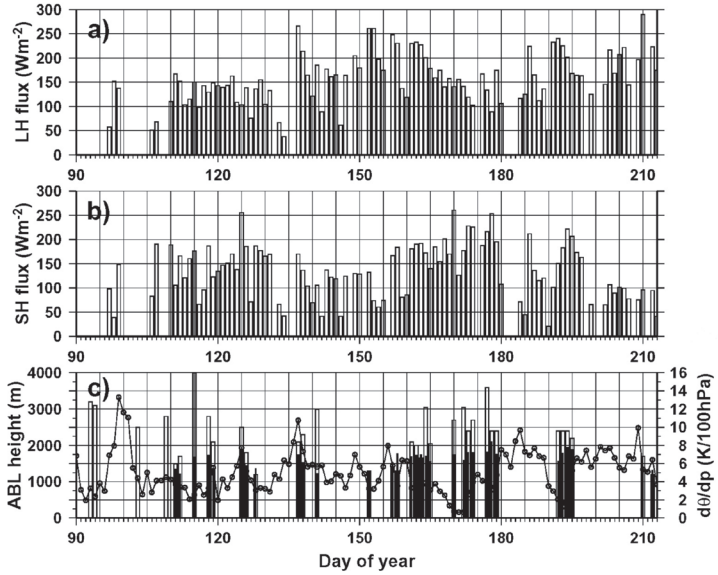

Figure 2
Day-to-day variation of **a)** daytime mean latent heat flux, **b)** daytime mean sensible heat flux at 12/32 m height, and **c)** diurnal maximum Z_i (open bars), Z_{ical} (solid bars), and the difference in the vertical gradient of potential temperature between 600 hPa and 700 hPa at 08 BST (00 UTC).

Numerical simulations of local circulation and cumulus generation over the Loess Plateau in China

Because the Loess Plateau consists of flat tablelands dissected by steep gullies, the topography has non-negligible effects on cumulus formation over the Plateau on the regional scale. Accordingly, ABL development was simulated numerically for clear days in which the cumulus-topped boundary layer grew to high altitudes. With the use of a cloud-resolving nonhydrostatic model, simulations were performed under two sets of bottom boundary conditions: actual and flat terrain. Some of the findings from the simulations can be summarized as follows. More cumulus clouds formed in the case with the actual terrain than in the case with flat terrain. Local circulation developed with horizontal and vertical scales of several kilometers over both the flat and real terrains. Over the flat terrain, the updrafts were distributed systematically and were characterized by Rayleigh–Bénard-type cellular convective structures; downdrafts emerged around the updrafts. In contrast, over the actual terrain, updrafts developed exclusively above the surface layer streaks that formed over the windward slopes and the edges of the tableland. Water vapor was lifted nonhomogeneously by local circulation on the windward slopes and the edges of the tableland (Figs. 3 and 4). As a result, development of cumulus clouds at the top of the ABL was evident only above these locations. Thus, the topography of the Loess Plateau significantly influences cumulus formation over the Plateau.

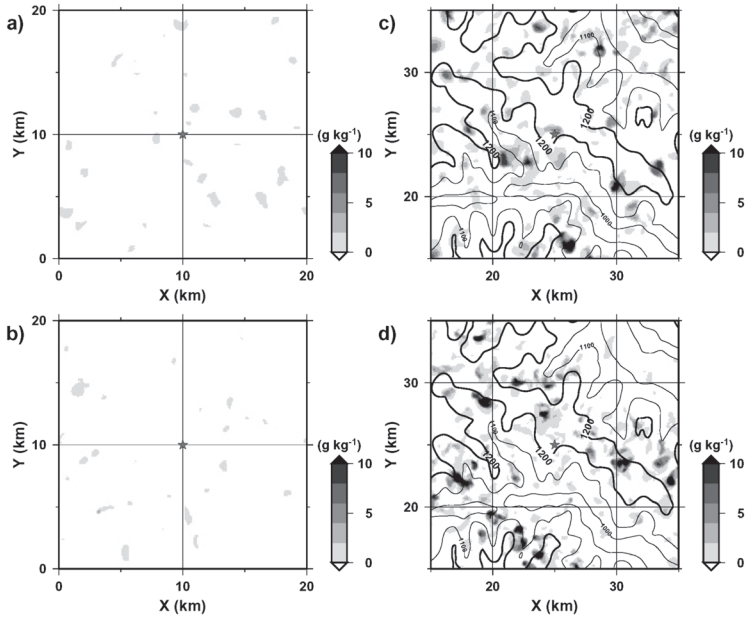

Figure 3 The distribution of vertically integrated cloud liquid water at 13 : 20 BST for the **a)** FLAT-DRY run, **b)** FLAT-WET run, **c)** ACTUAL-DRY run, and **d)** ACTUAL-WET run. The contour lines for the ACTUAL runs indicate every 100 m; the bold contour line indicates the flat tableland of 1200 m a.s.l.; the star indicates the location of the ABL observation site.

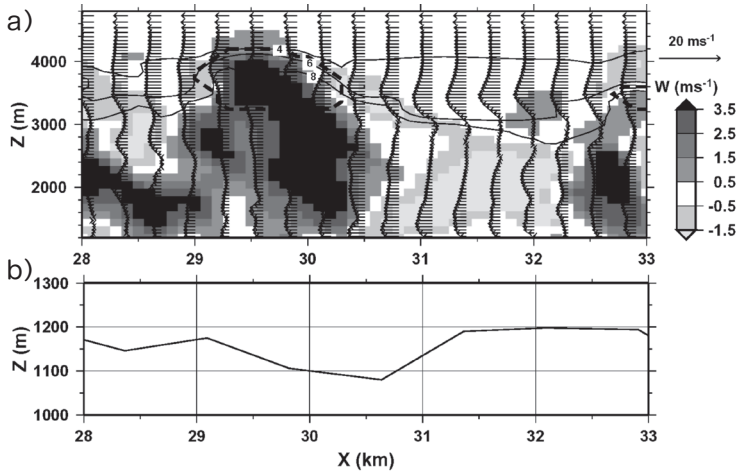

Figure 4
a) Cross section of vertical and horizontal wind velocity from 28 to 33 km (x axis) and 26 km (y axis) at 13 : 20 BST for the ACTUAL-DRY run (see Fig. 3). The gray scale indicates vertical wind, and the vectors indicate horizontal wind. The contour line indicates the mixing ratio of water vapor for every 2 g kg^{-1}. The bold dotted line indicates the cloud edge, defined as a mixing ratio of cloud liquid water of 1.0×10^{-4} g kg^{-1}.
b) Cross section of the altitude.

Laboratory of Ocean Climate Biology

The climate system surrounding us is governed by water and materials cycles in the hydrosphere and atmosphere on the Earth. In our laboratory, we aim in studying the inter-relationship between climate change and ocean biogeochemistry on time scales ranging from a decade to a century. A brief description of our laboratory's activities is as follows.

● Ocean Primary Productivity Monitoring by Satellites

Primary productivity is one of the key processes in understanding the relationship between climate change and ocean biogeochemistry. A global view of primary productivity can be attained by satellite remote sensing; however, its quantitative estimation is hindered by lack of ground-truth data on spatial and temporal scales. To fill this gap, we developed, as part of the Core Research for Evolutional Science and Technology (CREST) program "Project on Ocean Productivity Profiling System (POPPS)" during 1999–2004, an ocean productivity profiling system using an underwater profiling buoy system and a custom-made fast repetition rate fluorometer (FRRF). We are now developing a practical system for monitoring of ocean primary productivity by operating the productivity profiling system in combination with supporting data-handling systems to merge satellite and *in situ* data. This is under a new 5-year continuation project "Ocean Primary Productivity Monitoring by Satellites" as a part of Solution Oriented Research for Science and Technology (SORST), which began in 2004. The goal of the project is to design a system for monitoring global ocean primary productivity. The immediate task is to utilize satellite primary productivity data validated by the profiling buoy system for process studies on ocean biogeochemistry in response to physical forcing in order to demonstrate the usefulness of the validated satellite data.

Long-term operation of ocean productivity profiling system in central Sagami Bay

The underwater profiling buoy system is composed of an underwater winch system and a profiling buoy system. The profiling buoy is equipped with sensors, and normally deployed below the euphotic zone (EZ). It ascends to the surface on a preset schedule (once a day, at noon) and measures the vertical profile from the winch depth to the surface, and then returns to the winch to await the next cycle. A custom-made FRRF has been installed as the main sensor, in which data processing is performed in real time during the profiling measurements. All measured data are stored, with a part of the processed data being transmitted to the laboratory via a cellular phone when the buoy pops up to the surface. This instrument was in operation for almost a year, from November 2007 to November 2008, at observation station S3 in central Sagami Bay. Out of the 297 scheduled operations, 220 profiles were obtained successfully, with 152 completed real-time data transmissions. Data collected from the system are shown in Fig. 1 (Julian day 0 = January 1, 2008).

During winter, chlorophyll *a* (Chl*a*) concentration was low (< 0.5 mg m^{-3})

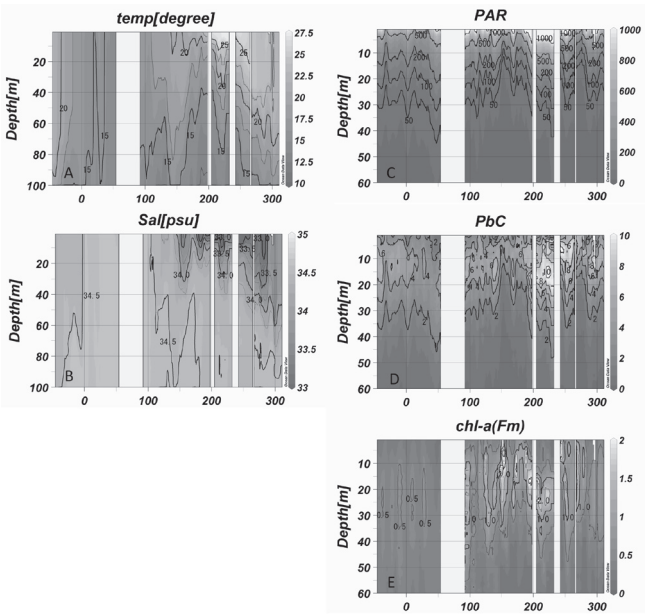

Fig. 1. Time-series data transmitted from the monitoring system in central Sagami Bay during November 2007 to November 2008. **(A)** Temperature (°C), **(B)** salinity (psu), **(C)** photosynthetically available radiation at noon (PAR; μE m^{-2} s^{-1}), **(D)** Chl*a*-specific gross productivity (Pbc; mgC mgChl^{-1} h^{-1}), and **(E)** maximum fluorescence (F_mD) corresponding to Chl*a* concentration.

within a well-mixed water column, and increased later with the development of stratification in the upper layer after April. Maximum Chl*a* conc. (> 2.0 mg m^{-3}) was found at 15–25 m depth during summer, which was deeper than the subsurface PbC maximum. This implied that photosynthetically produced particles (phytoplankton) are removed immediately from the upper layer and accumulate below. The peaks of PbC and Chl*a* did not appear exactly in parallel, which implied that subsequent processes such as grazing by zooplankton would partly control the phytoplankton biomass and primary productivity. This is the first ever long-term, continuous *in situ* measurement of ocean productivity, which demonstrates that our monitoring system showed promise in its ability to further understanding the natural variability of oceanic productivity.

Diurnal and seasonal variability in the physiological characteristics and productivity of marine phytoplankton in Sagami Bay

Biological processes of phytoplankton in the ocean could significantly influence the dynamics of the ecosystem such as the storage and cycles of carbon. These biological processes, including the productivity of phytoplankton, are subjected to environmental stress such as fluctuating temperature, salinity and irradiance. Under such varying conditions, photosynthetic strategies are most likely to occur to maintain productivity. The present study examined the diel and seasonal changes in physiological characteristics and productivity of phytoplankton using the FRRF in Sagami Bay, Japan.

Lower photochemical quantum efficiency (F_v/F_m) was observed at the surface in spring and the other seasons (Fig. 1). F_v/F_m measured at midday showed low values at the surface where PAR was the highest, mainly because of nonphotochemical quenching, and it increased sharply at depth (Fig. 2). F_v/F_0, an index indicating for photoinhibition (fraction of functional photosystem II reaction centers), also showed similar profiles and varied differently throughout the day. F_v/F_m and F_v/F_0 at the surface showed a clear diel pattern, with minimum values at around midday and maximum values at dusk and dawn (Fig. 2). This pattern was observed for all seasons, implying a common physiological strategy or mechanism. Comparing maximal F_v/F_m, relatively higher values were observed in spring and summer, indicating that the cells were in a better physiological state. F_v/F_0 was also observed to vary with the seasons. The decrease in the functional PSII reaction centers at the surface was as high as 80% in spring compared with around 40% in fall. In summer, with warmer and less saline water observed at the top layer of the water column, cells exihibited only a 30% decrease in F_v/F_0. In addition, reduction in the photosynthetic activity (PbC) was minimal during summer even at the surface. This suggested that the cells living in a better physical environment in summer were much more tolerant to high irradiance than those cells in spring and fall. Cells under high irradiance during the day and in the summer exhibited a photoacclimative strategy that permits continuous and uninterrupted photosynthesis by preventing photodamage. Such information on photosynthetic efficiency under varying environmental conditions is essential in quantifying primary productivity in the ocean.

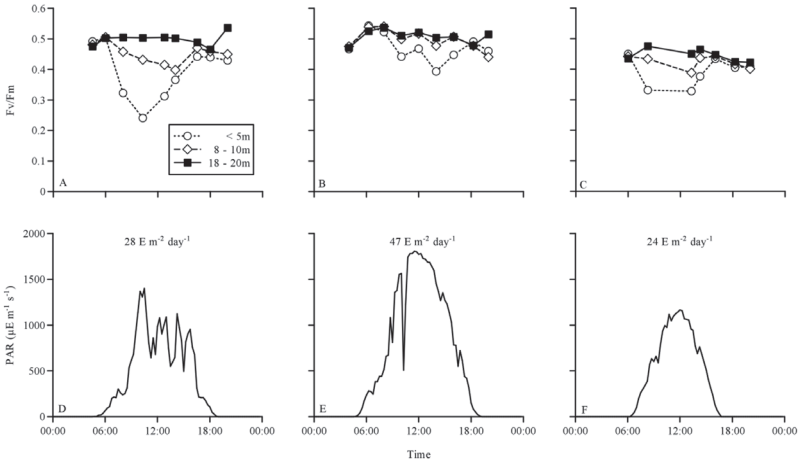

Fig. 2. Diel variability in F_v/F_m and surface PAR in spring (**A** & **D**), summer (**B** & **E**), and fall (**C** & **F**).

Laboratory of Bio-Physical Oceanography

Interannual variation in material transports through the eastern channel of the Tsushima Straits

Nutrient transports from the East China Sea into the Japan Sea through the Tsushima Straits play an important role in the nutrient budget and biological productivity of the southern part of the Japan Sea. In order to evaluate seasonal and interannual variations in material transports through the Tsushima Straits, we have conducted hydrographic observation across the eastern channel of the Tsushima Straits (ECTS) since 2005. We conducted observations twenty-three times along a single observation line.

Figure 1 shows volume, freshwater, and dissolved organic nitrogen (DIN) transports, respectively, averaged in August and September from 2005 to 2008. Each of these observed variables reached its maximum in 2005 and its minimum in 2007. Interannual variations in the volume, freshwater, and DIN transports indicate similar tendency: the variations in the freshwater and DIN transports seem to be associated with variations in the volume transport. However, although the volume transport in 2007 decreased by 29% from 2005, the freshwater and DIN transports in 2007 decreased by 49% and 63%, respectively, compared with those in 2005. Therefore, the variations in the freshwater and DIN transports are not adequately explained by the change of the volume transport alone.

Mean sea surface salinities in the ECTS in 2005 and 2007 were 31.31 and 33.37 psu, respectively. This result suggests that Changjiang discharge decreased in 2007, as most of the low-salinity water observed in the ECTS in summer originated in the Changjiang. In fact, Changjiang discharge, averaged from May to July in 2007, decreased by 19% compared to 2005. Considering the decrease rate of the volume transport and the river discharge, freshwater transport in 2007 is calculated to have been as $19.38 \times 10^6\,\mathrm{kg\,s^{-1}}$. This value coincides well with observed freshwater transport in 2007 of $17.25 \times 10^6\,\mathrm{kg\,s^{-1}}$. The low freshwater transport in 2007 is explained by the reduced volume transport and river discharge of the Changjiang. Meanwhile, mean DIN concentrations in the ECTS in 2005 and 2007 were 4.93 and 2.90 μM, respectively. Water temperature has high correlation with nutrient concentration, and the water temperatures in the lower layer at the central part of the ECTS in 2005 and 2008 were 16°C while those in 2006 and 2007 were 18°C. This difference of bottom water temperature might be related to the interannual variation in DIN transport.

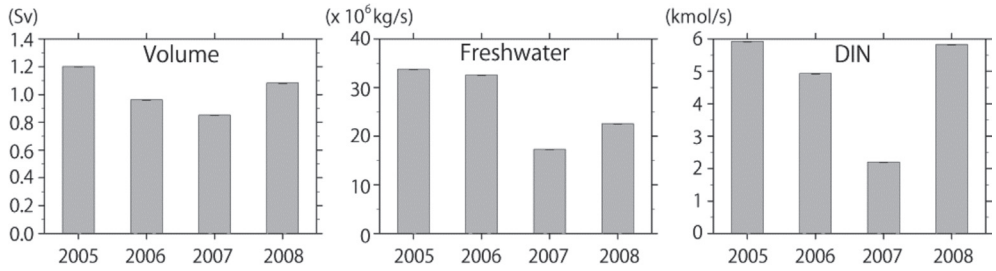

Fig. 1. Volume, freshwater, and DIN transports through the ECTS averaged in August and September from 2005 to 2008.

Enhancement of primary productivity in the southern East China Sea following episodic typhoon passage and its interannual variation

Enhancement of primary productivity (PP_{enh}) in the southern East China Sea (ECS) following typhoon passages was investigated using satellite data and a primary productivity (PP) model. A long-lasting southerly wind is important to push the Kuroshio shelfward, and the PP_{enh} following 16 typhoon passages was clearly observed to be associated with the variation in the shelfward movement of Kuroshio that generates upwelling of nutrients. Accordingly, we found

that the PP_{enh} was determined by typhoon translation speed (TS, $m\,s^{-1}$) and meridional wind (V, $m\,s^{-1}$) measured at Yonaguni Island, showing that the slower TS and the higher southerly wind, PP_{enh} would be higher (Figs. 2a and 2b). The importance of long-lasting southerly winds and the TS underlying PP_{enh} could be formulated empirically as an equation that could explain 88% of the variation in PP_{enh} (Fig. 2c). Applying this equation, we calculated that typhoon passages accounted for a minimum range of 0.6–11.8% of the ECS summer — fall new productivity (NP), with the lowest value in 1993 (due to only one typhoon passage) and the highest in 2001 (associated with 6 typhoon passages). These results suggest that typhoon passage over the southern ECS is an important phenomenon supporting NP in the ECS.

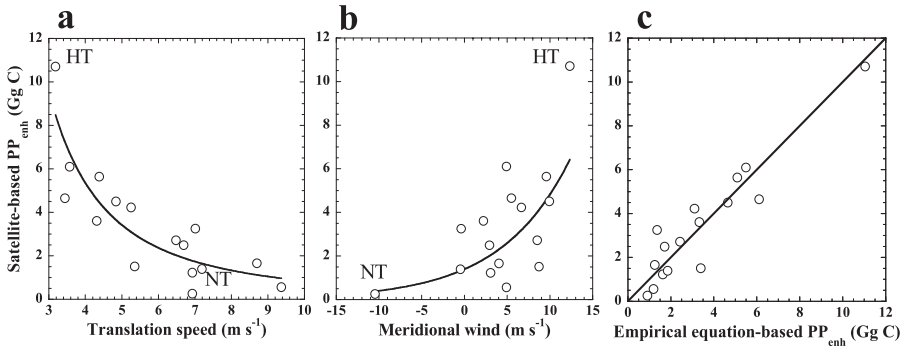

Fig. 2. Relationships between PP_{enh} and **(a)** TS ($R^2 = 0.76$), and **(b)** V ($R^2 = 0.45$). HT and NT are PP_{enh} by Typhoon Hai-Tang and Nock-Ten, respectively. Curves in **(a)** and **(b)** are non-linear regression lines. **(c)** Comparison between satellite-based and empirical equation-based PP_{enh} ($R^2 = 0.88$).

Short-term periodic decrease of water temperature in subsurface layer of Sagami Bay, Japan

Oceanographic conditions in Sagami Bay were investigated through an analysis of the POPPS buoy data. In the subsurface layer (> 150 m), water temperature frequently decreased regardless of the season (arrows in Fig. 3b), and strong eastward flows with speeds greater than 20 $cm\,s^{-1}$ simultaneously formed in the surface layer (< 150 m) (Fig. 3). These fluctuations in subsurface water temperature and surface flow had a period of 25–35 days, and particularly the flow fluctuation was closely related to variations of the Kuroshio axis south of Japan. These water temperature and flow fluctuations occurred together with (1) an upwelling of cold, deeper water in the subsurface layer and (2) an enhancement (or formation) of a cyclonic circulation in the surface layer in the northern part of Sagami Bay. These correlations indicate the presence of short-term periodic fluctuations in water temperature and flow fields of Sagami Bay, which are closely related to the Kuroshio axis variations south of Japan, and it is considered that these fluctuations are caused by a response of the density field to the flow field under geostrophic adjustment.

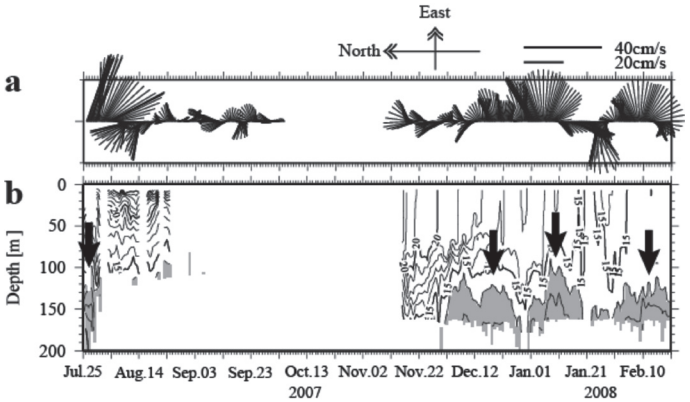

Fig. 3. **(a)** Vector stick plot of vertical mean low-passed filtered current between depths of 50 and 150 m and **(b)** depth-time plot of water temperature at depths of 0–200 m during a period from July 25, 2007 to February 20, 2008. Shaded areas in **(b)** represent water temperature with values less than 14°C. Contour intervals for water temperature are 1°C.

List of Publications

* : Staffs, students and research fellows in the HyARC.

1. Chiba, S., M.N. Aita, K. Tadokoro, T. Saino*, H. Sugisaki and K. Nakata
From climate regime shifts to lower-trophic level phenology: Synthesis of recent progress in retrospective studies of the western North Pacific. *Progress In Oceanography,* **77**, 112-126, 2008.
2. Eguchi, K., O. Abe and T. Hiyama*
Weight loss and isotopic shifts for water drops frozen on a liquid nitrogen surface. *Rapid Communications in Mass Spectrometry*, **22**, 3233-3237, 2008.
3. Endo, S.*, T. Shinoda*, H. Tanaka*, T. Hiyama*, K. Tsuboki*, H. Uyeda* and K. Nakamura*
Characteristics of vertical circulation in the convective boundary layer over the Huaihe River Basin in China in the early summer of 2004. *Journal of Applied Meteorology and Climatology,* doi: 10.1175/2008JAMC 1769.1, 2008. **47**(11), 2911-2928, 2008.
4. Fujiki, T., T. Hosaka, H. Kimoto, T. Ishimaru and T. Saino*
In situ observation of phytoplankton productivity by an underwater profiling buoy system: use of fast repetition rate fluorometry. *Marine Ecology Progress Series,* **l353**, 81-88, 2008.
5. Hirose, M.*, R. Oki, S. Shimizu, M. Kachi and T. Higashiuwatoko
Fine-scale diurnal rainfall statistics refined from 8 years of TRMM PR data. *Journal of Applied Meteorology and Climatology*, **47**(2), 544-561, 2008.
6. Islam, M.N. and H. Uyeda*
Vertical variations of rain intensity in different rainy periods in and around Bangladesh derived from TRMM observations. *International Journal of Climatology*, **28**(2), 273-279, 2008.
7. Kawase, H., T. Yoshikane, M. Hara, B. Ailikun, F. Kimura and T. Yasunari*
Downscaling of the climatic change in the rainband in East Asia by a Psedo Climate Simulation method. *Scientific Online Letters on the Atmosphere (SOLA)*, **4**, 73-76, doi: 10.2151/sola. 2008-019, 2008.
8. Liu, P., Y. Kajikawa, B. Wang, A. Kitoh, T. Yasunari*, T. Li, H. Annamalai, X. Fu, K. Kikuchi, R. Mizuta, K. Rajendran, D.E. Waliser and D. Kim
Tropical Intraseasonal Variability in the MRI-20km60L AGCM. *Journal of Climate,* DOI: 10.1175/2008JCLI2406.1, 2008.
9. Maeda, S., K. Tsuboki*, Q. Moteki, T. Shinoda*, H. Minda* and H. Uyeda*
Detailed Structure of Wind and Moisture Fields around the Baiu Frontal Zone over the East China Sea. *Scientific Online Letters on the Atmosphere (SOLA)*, **4**, 141-144, doi: 10.2151/sola. 2008-036, 2008.
10. Masunaga, H.*, M. Satoh and H. Miura
A Joint Satellite and Global Cloud-Resolving Model Analysis of a Madden-Jullian Oscillation Event: Model Diagnosis. *Journal of Geophysical Research*, **113**, D17210, doi: 10.1029/2008JD009986, 2008.
11. Minda, H.*, F. A. Furuzawa*, S. Satoh and K. Nakamura*
Bird migration echoes observed by polarimetric radar. *IEICE*, E91-B, **6**, 2085-2089, 2008.
12. Miyazaki, C. and T. Yasunari*
Dominant interannual and decadal variability of winter surface air temperature over Asia and the surrounding oceans. *Journal of Climate*, **21**(6), 1371-1386, 2008.
13. Moteki, Q., R. Shirooka, H. Kubota, T. Ushiyama, K.K. Reddy, K. Yoneyama, M. Katsumata, N. Sato, K. Yasunaga, H. Yamada, B. Geng, M. Fujita, M. Yoshizaki, H. Uyeda* and T. Chuda
Mechanism of the northward propagation of mesoscale convective systems observed on 15 June 2005 during PALAU2005. *Journal of Geophysical Research,* **113**, D14126, doi: 10.1029/2008JD009793, 2008.
14. Nishikawa, M.*, T. Hiyama*, K. Tsuboki* and Y. Fukushima
Numerical simulations of local circulation and cumulus generation over the Loess Plateau, China. *Journal of Applied Meteorology and Climatology,* doi: 10.1175/JAMC2041.1, 2008.
15. Ohta, T., T.C. Maximov, A.J. Dolman, T. Nakai, M.K. van der Molen, A.V. Kononov, A.P. Maximov, T. Hiyama*, Y. Iijima, E.J. Moors, H. Tanaka*, T. Toba and H. Yabuki
Interannual variation of water balance and summer evapotranspiration in an eastern Siberian larch forest over a 7-year period (1998-2006). *Agricultural and Forest Meteorology,* **148**, 1941-1953, 2008.

16. Pham, N.T.*, K. Nakamura*, F.A. Furuzawa* and S. Satoh
Characteristics of Low Level Jets over Okinawa in the Baiu and post-Baiu Seasons revealed by Wind Profiler Observations. *Journal of the Meteorological Society of Japan*, **86**(5), 699-717, 2008.

17. Prasanna, V.* and T. Yasunari*
Interannual variability of atmopsheric water balance over south Peninsular India and Sri Lanka during northeast monsoon season. *International Journal of Climatology,* **28**(15), 1997-2009, doi: 10.1002/joc.1683, 2008.

18. Rao, T.N., N.V.P. Kirankumar, B. Radhakrishna, D.N. Rao and K. Nakamura*
Classification of Tropical Precipitating Systems Using Wind Profiler Spectral Moments: 1. Algorithm Description and Validation. *Journal of Atmospheric and Oceanic Technology,* **25**(6), 898-908, 2008.

19. Rao, T.N., N.V.P. Kirankumar, B. Radhakrishna, D.N. Rao and K. Nakamura*
Classification of Tropical Precipitating Systems Using Wind Profiler Spectral Moments: 2. Statistical characteristics of rainfall systems and sensitivity analysis. *Journal of Atmospheric and Oceanic Technology,* **25**(6), 884-897, 2008.

20. Renfrew, I.A., G.W.K. Moore, J.E. Kristjansson, H. Olafsson, S.L. Gray, G.N. Petersen, K. Bovis, P.R.A. Brown, I. Fore, T. Haine, C. Hay, E.A. Irvine, A. Lawrence, T. Ohigashi*, S. Outten, R.S. Pickart, M. Shapiro, D. Sproson, R. Swinbank, A. Woolley and S. Zhang
The Greenland Flow Distortion experiment. *Bulletin of the American Meteorological Society,* **89**(9), 1307-1324, 2008.

21. Sato, T., T. Yoshikane, M. Satoh, H. Miura and H. Fujinami*
Resolution dependency of the diurnal cycle of convective clouds over the Tibetan Plateau in a mesoscale model. *Journal of Meteorological Society of Japan*, **86A**, 17-31, 2008.

22. Shimizu, S., H. Uyeda*, Q. Moteki, T. Maesaka, M. Takaya, K. Akaeda, T. Kato and M. Yoshizaki
Structure and formation mechanism of 24 May 2000 supercell-like thunderstorm observed over Kanto plain, Japan. *Monthly Weather Review,* **136**(7): 2389-2407, 2008.

23. Siswanto, E.*, H. Nakata, Y. Matsuoka, K. Tanaka, Y. Kiyomoto, K. Okamura, J. Zhu and J. Ishizaka
The long-term freshening and nutrient increases in summer surface water in the northern East China Sea in relation to Changjiang discharge variation. *Journal of Geophysical Research*, **113**, 2008.

24. Siswanto, E.*, J. Ishizaka, A. Morimoto*, K. Tanaka, K. Okamura, A. Kristijono and T. Saino*
Ocean physical and biogeochemical responses to the passage of Typhoon Meari in the East China Sea observed from Argo float and multiplatform satellites. *Geophysical Research Letters,* **35**, 2008.

25. Takahashi, A., T. Hiyama*, M. Nishikawa*, H. Fujinami*, A. Higuchi, W. Li, W. Liu and Y. Fukushima
Diurnal variation of water vapor mixing between the atmospheric boundary layer and free atmosphere over Changwu, the Loess Plateau in China. *Scientific Online Letters on the Atmosphere (SOLA),* **4**, 33-36, 2008.

26. Takahashi, C., H. Uyeda*, M. Maki, K. Iwanami and R. Misumi
Relationships among Structures, Development Processes, and Heating Profiles for Two Mesoscale Convective Systems in Inactive Phase of a Large-Scale Disturbance over Northern Australia during the Southern Summer in 1998-1999. *Journal of the Meteorological Society of Japan*, **86**(1), 81-117, 2008.

27. Takahashi, H.G., T. Yoshikane, M. Hara and T. Yasunari*
High-resolution regional climate simulations of the long-term decrease in September rainfall over Indochina. *Atmospheric Science Letters,* **10**(1), 14-18, doi: 10.1002/asl. 203, 2008.

28. Takikawa, T., A. Morimoto*, G. Onitsuka, A. Watanabe* and M. Moku
Characteristics of Water Mass under the Surface Mixed Layer in Tsushima Straits and the Southwestern Japan Sea in Autumn. *Journal of Oceanography,* **64**(4), 585-594, 2008.

29. Tanaka, H.*, T. Hiyama* and K. Nakamura*
Turbulent flux observations at the tip of a narrow cape on Miyako Island in Japan's Southwestern Islands. *Journal of the Meteorological Society of Japan*, **86**(5), 649-667, 2008.

30. Tanaka, H.*, T. Hiyama*, N. Kobayashi, H. Yabuki, Y. Ishii, R.V. Desyatkin, T.C. Maximov and T. Ohta
Energy balance and its closure over a young larch forest in eastern Siberia. *Agricultural and Forest Meteorology*, **148**, 1954-1967, 2008.

31. Tangang, F.T., L. Juneng, E. Salimun, P.N. Vinayachandran, Y.K. Seng, C.J.C. Reason, S.K. Behera and T. Yasunari*
On the roles of the northeast cold surge, the Borneo vortex, the Madden-Julian Oscillation, and the Indian Ocean Dipole duringthe extreme 2006/2007 flood in southern Peninsular Malaysia. *Geophysical Research Letters*, **35**, L14S07, doi: 10.1029/2008GL033429, 2008.

32. Tsuboki, K.*
High-Resolution Simulations of High-Impact Weather Systems Using the Cloud-Resolving Model on the Earth Simulator. *High Resolution Numerical Modelling of the Atmosphere and Ocean,* Hamilton, Kevin; Ohfuchi, Wataru (Eds.), Springer New York, 141-156. 2008.

33. Uyeda*, H.
Mesoscale Precipitation Systems Along the Meiyu/Baiu Front and Future Expectation for Research Radar and Weather Radar Network. *Journal of Disaster Research*, **3**(1), 61-68, 2008.

34. Yamamoto, K.M., F.A. Furuzawa*, A. Higuchi and K. Nakamura*
Comparison of diurnal variations in precipitation systems observed by TRMM PR, TMI, and VIRS. *Journal of Climate*, **21**(16), 4011-4028, 2008.

Hydrospheric Atmospheric Research Center (HyARC)

Nagoya University

Furo-cho, Chikusa-ku, Nagoya 464-8601, Japan

Office:

Telephone: +81-52-789-3466

Facsimile: +81-52-789-3436

Home Page: http://www.hyarc.nagoya-u.ac.jp/hyarc/

The 2008 Annual Report was published July 2009 by the Hydrospheric Atmospheric Research Center (HyARC) Nagoya University. Copies of this report are available from the office of the Center.

Printed by Nagoya University COOP


HyARC
Hydrospheric Atmospheric Research Center, Nagoya University